Late Cretaceous tectonic history of the Sierra-Salinia-Mojave arc as recorded in conglomerates of the Upper Cretaceous and Paleocene Gualala Formation, northern California

Ronald C. Schott[1] and Clark M. Johnson

Department of Geology and Geophysics, University of Wisconsin-Madison, Madison, Wisconsin, USA

James R. O'Neil

Department of Geological Sciences, University of Michigan, Ann Arbor, Michigan, USA

[1] Upper Cretaceous and Paleogene conglomerates in the Gualala basin of northern California likely preserve the westernmost record of sedimentation in California during the interval between cessation of Sierran batholith magmatism and inception of Neogene transform activity on the San Andreas fault system. Detailed chemical and H, O, Sr, Nd, and Pb isotope analyses of conglomerate clasts, as well as U/Pb zircon ages, identify two source types: (1) evolved granite, like those found in the Salinian block or eastern Sierra Nevada batholith, and (2) primitive oceanic arcs that were restricted to the western portions of the Mesozoic arc system. The provenance of the Gualala clasts can be entirely explained through derivation from the Sierra-Salinian-Mojave portion of the Mesozoic Cordilleran arc, and do not support models for extensive large-scale translation of the basin from low latitudes along a pre-Neogene transform fault system. Contemporaneous deposition of the contrasting lithologies in the Gualala basin is interpreted to reflect tectonic juxtaposition of the source terranes approximately 80 m.y. ago. Tectonic processes responsible for juxtaposition of the two source regions in the Late Cretaceous most probably involved zones of lithospheric weakness that later localized the San Andreas fault system in the Neogene. Chemical, isotopic, and age data tie the Gualala basin to North American continental basement in the Mojave-Salinian segment of the Mesozoic Cordilleran arc and imply minimal pre-Neogene translation of the basin contrary to the low latitude origin for the basin inferred from previous paleomagnetic and paleontologic studies. *INDEX TERMS:* 1035 Geochemistry: Geochronology; 1040 Geochemistry: Isotopic composition/chemistry; 1065 Geochemistry: Trace elements (3670); 8105 Tectonophysics: Continental margins and sedimentary basins (1212); *KEYWORDS:* isotope, provenance, cordillera

1. Introduction

[2] Sedimentary basins in orogenic belts record tectonic events that may manifest themselves on the surface, which may be distinct from those that are preserved in deep crustal environments. In some cases, sedimentary basins may record the effects of large-scale translation of exotic terranes [e.g., *Cowan*, 1994; *Dickinson and Butler*, 1998]. Many exotic terranes of western North America have demonstrable and well-accepted post-Cretaceous displacements of tens to hundreds of kilometers with respect to cratonic North America. More controversial are interpretations of thousands of kilometers of displacement suggested by some paleomagnetic and paleontologic studies [e.g., *Kanter and Debiche*, 1985; *Elder et al.*, 1998]. A significant unresolved aspect of the latter hypotheses is the documentation of faults along which such large displacements could be accommodated.

[3] The Gualala basin offers a unique opportunity to address the tectonic evolution of the Cordillera of California and of the role of the faults that offset it. Currently situated adjacent to the San Andreas fault in northern California (Figure 1), the basin is clearly offset from its location of origin by motion along the San Andreas fault system in the Neogene [e.g., *Ross*, 1984; *Graham et al.*, 1989; *Powell*, 1993]. Pre-Neogene translation may have occurred as well. Some workers have suggested that the basin was originally located hundreds of kilometers south of its current position

[1]Now at Department of Geology and Physics, Lake Superior State University, Sault Sainte Marie, Michigan, USA.
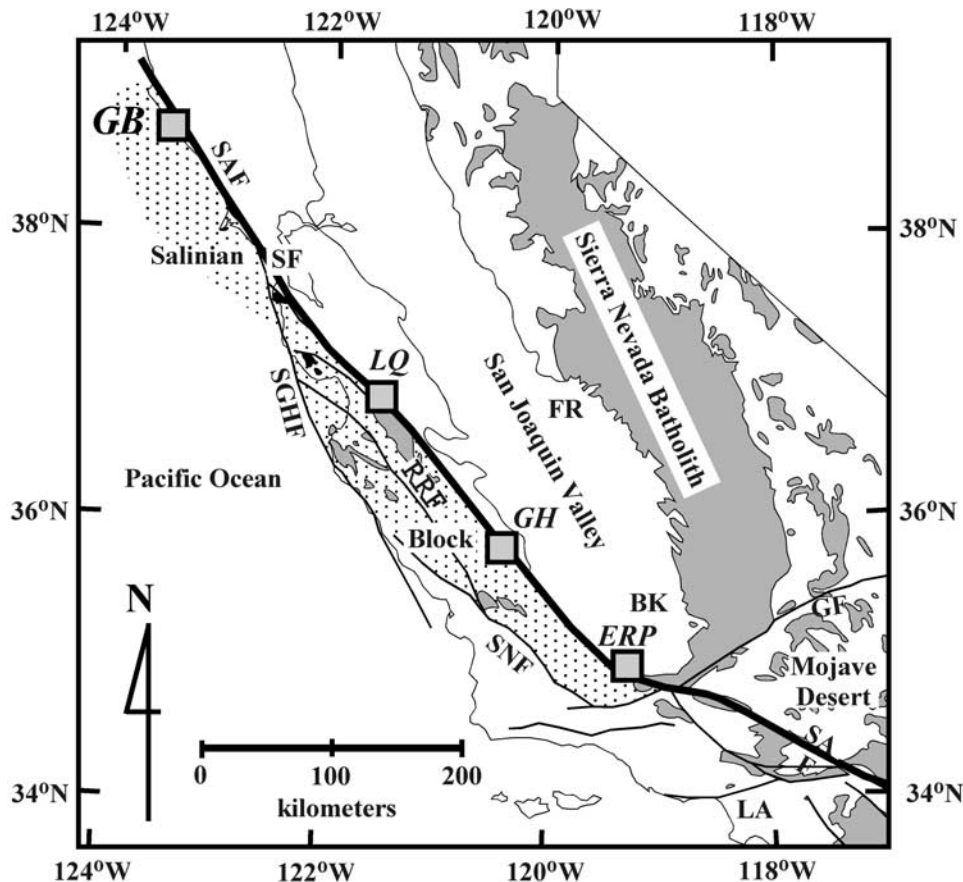
Figure 1. Current location in California of the displaced Salinian block (stippled pattern) and Gualala basin (GB), as well as the Eagle Rest Peak (ERP) mafic basement terrane and its offset counterparts at Gold Hill (GH) and Logan Quarry (LQ). Faults: SAF, San Andreas fault; GF, Garlock Fault; SGHF, San Gregorio-Hosgri fault; RRF, Reliz-Rinconada fault; SNF, Sur-Nacimiento fault. Cities: SF, San Francisco; LA, Los Angeles; FR, Fresno; BK, Bakersfield.

and adjacent to the northern Salinian block and southern San Joaquin Valley [e.g., *Wentworth*, 1966; *Ross et al.*, 1973; *Kistler et al.*, 1973; *James et al.*, 1993; *Schott and Johnson*, 1998a, 1998b, 2001], while others place it thousands of kilometers south of its current position [e.g., *Kanter and Debiche*, 1985; *Elder et al.*, 1998]. Detailed discussions of the contrasting hypotheses for the origin of the basin are presented by *Burnham* [1998] and *Schott* [2000].

[4] Because the sedimentary record of the Gualala basin spans almost 30 m.y. during the Late Cretaceous and early Paleogene, sedimentary debris within it record pre-Neogene tectonic events. In this paper we present new geochemical and isotopic data that bear on the provenance of conglomerate clasts from the Gualala Formation. These clasts are of two types, gabbroic and rhyolitic/granitic, in places mixed together in the same beds. The present study encompasses both the gabbroic clasts that have been the focus of study by previous workers [*Ross*, 1970; *Ross et al.*, 1973; *Kistler et al.*, 1973; *James et al.*, 1993], as well as rhyolitic and granitic clasts [*Schott and Johnson*, 1998a], which have received less attention. The focus here is on the Late Cretaceous to Paleocene section and is complemented by previous work on the overlying Eocene German Rancho Formation [*Schott and Johnson*, 2001]. New data are also presented for the mafic basement terrane at Eagle Rest

Peak (ERP) and its outliers at Gold Hill (GH) and Logan Quarry (LQ), rocks that have been debated as possible source materials for mafic conglomerate clasts at Gualala. Identifying these sources would independently constrain offset on the San Andreas fault in central California [*Ross*, 1970; *Ross et al.*, 1973; *Kistler et al.*, 1973; *James et al.*, 1993].

2. Depositional Setting and Age

[5] Upper Cretaceous and early Tertiary sedimentary rocks in the Gualala basin include conglomerates, sandstones and mudstones that were deposited as a turbidite fan-channel complex at bathyal depths in a forearc tectonic setting [*Wentworth*, 1966; *Loomis and Ingle*, 1994]. *Wentworth* [1966] assigned Upper Cretaceous and lowest Paleocene rocks to the Gualala Formation and subdivided it into two members on the basis of conglomerate clast and sandstone composition (Figure 2). The Stewarts Point Member is characterized by felsic volcanic and plutonic clasts in a matrix of K-feldspar arkose, whereas the Anchor Bay Member contains a mafic clast assemblage in a plagioclase arkose (<5% K-feldspar) [*Wentworth*, 1966]; the two members are interfingered and hybrid felsic-mafic conglomerate clast suites occur near their mapped contacts.
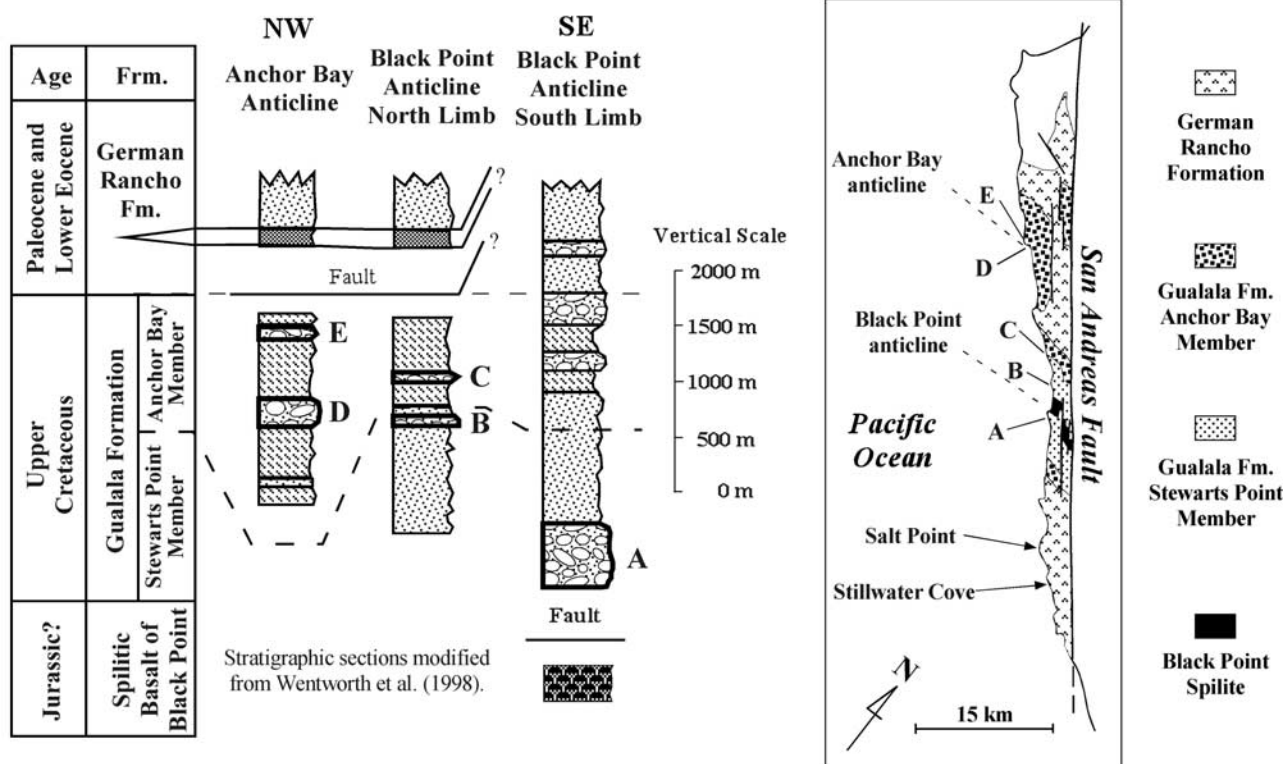
Figure 2. Generalized geologic map and stratigraphic section of the Gualala Formation (modified from *Wentworth et al.* [1998]). Conglomerate sample locality key: A, Black Point (KCGR clasts only); B, Smuggler's Cove (KCGR clasts only); C, Sea Ranch Stable/Pebble Beach (interfingered and hybrid conglomerate beds, KCGR and JOGD clasts); D, Anchor Bay (JOGD clasts only); E, Havens Neck (JOGD clasts only). Localities and lithologies for clasts are given in Table 1.

The Upper Cretaceous section sits structurally above spilitic basalt of uncertain tectonic affinity [*Phillips et al.*, 1998], and *Wentworth et al.* [1998] conclude that the contact between these units is a low angle or "detachment" fault. Stratigraphically above the Gualala Formation lies the Paleocene to lower Eocene German Rancho Formation (Figure 2), another section of turbidites that are dominated by K-feldspar arkose and contain conglomerates of markedly different composition [*Schott and Johnson*, 2001].

[6] Microfossils and sparse macrofossils constrain a Campanian age for the lowest Stewarts Point strata and a Maastrichtian age for the majority of the section [*Loomis and Ingle*, 1994; *Elder et al.*, 1998; *Wentworth et al.*, 1998]. Conglomerates in the uppermost Anchor Bay Member contain clasts and fragments of Late Cretaceous, shallow water macrofossils [*Elder et al.*, 1998] in a matrix that contains Paleocene foraminifera [*McDougall*, 1998], suggesting that Gualala Formation sedimentation spanned the Cretaceous-Tertiary boundary.

3. Results

[7] Chemical and isotopic compositions were determined on whole rock samples of conglomerate clasts, and U/Pb zircon ages were determined on zircons separated from the clasts, following methods discussed by *Schott* [2000]. Tables 1–4 provide sample localities, interpreted ages, and rock descriptions (Table 1), U/Pb zircon ages (Table 2),

chemical analyses (Table 3), and isotopic compositions (Table 4).

3.1. Upper Cretaceous Conglomerate Clasts

[8] Upper Cretaceous conglomerate clasts can be broadly subdivided into two suites that are judged to be continental or oceanic on the basis of their age and isotopic compositions. This source distinction corresponds to the compositional and mapped field designation of the Stewarts Point and Anchor Bay Members of the Gualala Formation as originally delineated by *Wentworth* [1966]. Clasts of continental origin (designated KCGR) are most commonly rhyolitic or granitic (often porphyritic) and have a range of mid-Cretaceous crystallization ages, and their isotopic compositions suggest an origin on the eastern (continental) side of the Cretaceous magmatic arc of California. In contrast, clasts of oceanic origin (designated JOGD) have gabbroic to quartz diorite compositions, Late Jurassic crystallization ages, and isotopic compositions that are characteristic of an oceanic source.

3.1.1. Ages

[9] U/Pb age systematics of zircon from KCGR clasts are complex and indicate a significant amount of inherited (Precambrian?) Pb in some zircons, as well as Pb loss (Table 2). None of the zircon fractions from the KCGR clasts yield concordant ages (Figure 3), where inherited Pb is both a major (samples KCGR-1, KCGR-8, and KCGR-11) and a minor (samples KCGR-4, KCGR-9, and KCGR-15) compo-

Table 1a. Upper Cretaceous Gualala Formation Conglomerate Clast Sample Localities, Interpreted Ages, and Petrography

Sample	Field Sample	Latitude North	Longitude West	Locality	Interpreted U/Pb Zircon Crystallization Age,[b] Ma	Rock Classification and Texture[a]
Jurassic Oceanic Gabbro and Diorite Clasts (JOGD)						
JOGD-1	CJ-826-1A	38°48′38″	123°35′49″	Haven's Neck	150[b]	qtz hbd gabbro
JOGD-2	CJ-826-1C	38°48′38″	123°35′49″	Haven's Neck	150[b]	hbd cpx gabbro
JOGD-3	RS92GU5	38°48′08″	123°34′58″	Anchor Bay	150[b]	hbd qtz gabbro
JOGD-4	RS96GU2	38°48′08″	123°34′58″	Anchor Bay	150[b]	hbd qtz gabbro
JOGD-5	RS92SP2	38°43′33″	123°28′54″	Shell Beach	145 ± 1	hbd qtz gabbro
JOGD-6	RS92SP13	38°43′33″	123°28′54″	Shell Beach	150[b]	mus biot granodiorite
JOGD-7	RS92SP14	38°43′33″	123°28′54″	Shell Beach	150[b]	cpx gabbro
JOGD-8	RS92SP16	38°43′33″	123°28′54″	Shell Beach	145 +1/−4	hbd qtz cpx gabbro
JOGD-9	RS92SP26	38°43′33″	123°28′54″	Shell Beach	158.5 ± 0.5	hbd qtz cpx gabbro
JOGD-10	CJ-829-2A	38°43′23″	123°28′31″	Knipp	150[b]	cpx gabbro
JOGD-11	CJ-829-2D	38°43′21″	123°28′29″	Knipp	150[b]	hbd qtz gabbro
JOGD-12	CJ-829-3A	38°43′34″	123°28′45″	Knipp	150[b]	hbd qtz gabbro
JOGD-13	RS92SP27	38°42′46″	123°27′25″	Sea Ranch Stable	150[b]	hbd qtz gabbro
JOGD-14	RS92SP30	38°42′46″	123°27′25″	Sea Ranch Stable	144 ± 2	hbd gabbro
JOGD-15	RS92SP31	38°42′46″	123°27′25″	Sea Ranch Stable	150[b]	hbd gabbro
JOGD-16	RS92SP32	38°42′46″	123°27′25″	Sea Ranch Stable	150[b]	hbd qtz gabbro
JOGD-17	ABc-1	NR	NR	Anchor Bay	150[b]	hbd qtz gabbro
JOGD-18	SR-3	NR	NR	Sea Ranch Stable	150[b]	hbd qtz gabbro
Cretaceous Continental Granite and Rhyolite Clasts (KCGR)						
KCGR-1	RS92SP15	38°43′33″	123°28′54″	Shell Beach	85 ± 5	hbd biot granodiorite
KCGR-2	CJ-829-3A	38°43′34″	123°28′45″	Knipp	100[b]	hbd biot granodiorite
KCGR-3	CJ-829-4B	38°43′25″	123°28′33″	Knipp	100[b]	equigranular hbd biot granite
KCGR-4	RS92SP40	38°42′46″	123°27′24″	Sea Ranch Stable	101 ± 1	equigranular hbd biot granite
KCGR-5	RS92SP42	38°42′12″	123°26′49″	Smuggler's Cove	100[b]	biot granite
KCGR-6	RS92SP43	38°42′12″	123°26′49″	Smuggler's Cove	100[b]	biot granite
KCGR-7	RS92SP45	38°42′13″	123°26′49″	Smuggler's Cove	101 ± 2	biot granite
KCGR-8	RS92SP54	38°42′12″	123°26′49″	Smuggler's Cove	100[b]	rhyolite
KCGR-9	RS92SP6	38°40′44″	123°25′51″	Black Point	125 ± 4	biot granite
KCGR-10	RS92SP7	38°40′44″	123°25′51″	Black Point	100[b]	medium-grained, equigranular biot granite
KCGR-11	RS92SP8	38°40′44″	123°25′50″	Black Point	100 ± 5	biot granite
KCGR-12	RS92SP10	38°40′44″	123°25′50″	Black Point	100[b]	rhyolite
KCGR-13	RS92SP55	38°40′55″	123°26′01″	Black Point	97 ± 2	coarse-grained, equigranular biot granite
KCGR-14	RS92SP56	38°40′55″	123°26′01″	Black Point	100 ± 2	coarse-grained, equigranular biot granite
KCGR-15	RS92SP58	38°40′55″	123°26′01″	Black Point	106 ± 2	biot granite
KCGR-16	RS92SP60	38°40′55″	123°26′01″	Black Point	100[b]	biot granite
KCGR-17	RS92SP62	38°40′55″	123°26′01″	Black Point	95 ± 2	biot granite
KCGR-18	RS92SP70	38°40′55″	123°26′01″	Black Point	98 ± 2	coarse-grained, equigranular biot granite

[a]Texture of JOGD clasts is medium-grained, equigranular unless otherwise noted. Texture of KCGR clasts is porphyritic with aphanitic groundmass unless otherwise noted. Varietal minerals listed in order of increasing abundance. Abbreviations are biot, biotite; cpx, clinopyroxene; hbd, hornblende; qtz, quartz.

[b]Assumed age is based on dated clasts of similar composition and texture; there is insufficient zircon yield for U/Pb age determination.

nent. In contrast, two other samples (KCGR-13 and KCGR-18) yield near-concordant fractions (Figure 3) that have a wide range of $^{238}U/^{206}Pb^*$ ages (5–11 m.y.). The zircon fractions from these two clasts have high U contents (1000–1400 ppm U) and have lost Pb. Crystallization ages of the provenance terrane(s) span a broad range of the mid-Cretaceous (circa 125 Ma to circa 85 Ma), although a majority of rocks appear to have crystallized around 100 ± 5 Ma. The average age of 100 Ma corresponds to the time of a major magmatic pulse in the California batholiths [e.g., *Stern et al.*, 1981; *Chen and Moore*, 1982; *Saleeby et al.*, 1987; *James*, 1992].

[10] Four of the JOGD clasts yielded sufficient zircon for U/Pb age determinations (Table 2), and these clasts comprise relatively evolved quartz-bearing gabbros or diorites that might also be characterized as mafic tonalites. Three of these clasts (JOGD-5, JOGD-8, and JOGD-14) have multiple concordant or near concordant fractions that imply crystallization ages at or near the Jurassic-Cretaceous boundary (144 ± 2 Ma) (Figure 4a). Zircons from the fourth clast (JOGD-9) yielded a single concordant age of 158.5 ± 1 Ma.

James et al. [1993] previously dated three mafic clasts from the Anchor Bay area that yielded slightly discordant zircon fractions that have $^{238}U/^{206}Pb^*$ ages ranging from 147 to 165 Ma; two of these clasts were nearly concordant at 162 to 165 Ma. *James et al.* [1993] interpreted their ages to be minimum ages, on the basis of the implicit assumption that uncertainties in age estimates are more likely to reflect Pb loss rather than inheritance in the mafic samples. Although it is possible that all of the circa 145 Ma zircon fractions dated in this study represent Pb loss from a circa 160 Ma crystallization age, we feel that the clustering of ages at circa160-165 and circa 145 Ma reflects a true bimodal age distribution for gabbroic rocks within the provenance terrane. This age distribution is similar to that observed in the Coast Range Ophiolite (CRO) [*Hopson et al.*, 1981]. The lack of significant inherited components for the JOGD clasts is consistent with their oceanic character (below).

3.1.2. Petrography and Geochemistry

[11] Major element compositions of the KCGR clasts reflect the highly evolved nature of their source bodies (Table 3); many KCGR clasts have >75 wt % SiO_2. Because

Table 1b. New Samples From the Mafic Basement Terrane at Eagle Rest Peak, Gold Hill, and Logan Quarry: Sample Localities, Interpreted Ages, and Petrography

Sample	Field Sample	Latitude North	Longitude West	Interpreted U/Pb Zircon Crystallization Age, Ma	Rock Classification and Texture[a]
			Eagle Rest Peak (ERP)		
ERP-1	RS92ER1	34°55′36″	119°14′57″	>160[b]	fine-grained amphibolite
ERP-2	CJ-40A	34°56′19″	119°12′07″	160[c]	fine-grained websterite
ERP-3	CJ-41A	34°56′16″	119°12′38″	160[c]	hbd gabbronorite
ERP-4	CJ-41A-A	34°56′16″	119°12′38″	160[c]	hbd gabbro
ERP-5	CJ-42A	34°57′01″	119°13′24″	160[c]	ol gabbro
ERP-6	CJ-42B	34°57′01″	119°13′24″	160[c]	anorth gabbro
ERP-7	CJ-43A	34°56′37″	119°13′49″	160[c]	hbd qtz gabbro
ERP-8	CJ-43C	34°56′37″	119°13′49″	160[c]	qtz hbd gabbro
ERP-9	RS92ER2	34°56′15″	119°12′28″	160[c]	hbd gabbro
ERP-10	RS92ER9	34°56′22″	119°12′05″	160[c]	foliated hbd cpx gabbro
ERP-11	RS92ER15	34°56′07″	119°13′12″	159 ± 2	hbd qtz gabbro
ERP-12	RS92ER18	34°55′34″	119°14′25″	160[c]	websterite
ERP-13	RS92ER28	34°56′43″	119°13′47″	160[c]	hbd cpx gabbro
ERP-14	RS92SC1	34°55′47″	119°16′09″	157 +4/−1	hbd tonalite
ERP-15	RS92SC7	34°55′41″	119°16′35″	160[c]	hbd tonalite
ERP-16	CJ-40B	34°56′19″	119°12′07″	160[c]	qtz vein
ERP-17	CJ-42BQ	34°57′01″	119°13′24″	160[c]	qtz vein
ERP-18	DR-1169A	NR	NR	160[c]	hbd qtz gabbro
ERP-19	DR-1161C	NR	NR	160[c]	hbd qtz gabbro
			Gold Hill (GH)		
GH-1	CJ-21	35°49′48″	120°21′00″	160[c]	cpx hbd qtz gabbro
GH-2	CJ-22	35°49′43″	120°21′01″	160[c]	hbd qtz gabbro
GH-3	CJ-24	35°49′38″	120°20′57″	160[c]	hbd qtz gabbro
GH-4	CJ-25	35°49′37″	120°20′55″	160[c]	hbd qtz gabbro
GH-5	CJ-27	35°49′33″	120°20′54″	160[c]	hbd qtz gabbro
GH-6	CJ-28	NR	NR	160[c]	cpx hbd qtz gabbro
GH-7	CJ-29	NR	NR	160[c]	hbd qtz gabbro
GH-8	SH-4	NR	NR	160[c]	hbd qtz gabbro
GH-9	CJ-GH-1	NR	NR	160[c]	hbd qtz gabbro
GH-10	RS92CV5	35°49′48″	120°20′53″	160[c]	hbd qtz gabbro
GH-11	RS92CV6	35°49′45″	120°20′56″	160 ± 1	hbd qtz gabbro
GH-12	CJ-24V	35°49′38″	120°20′57″	160[c]	qtz vein
GH-13	CJ-25VA	35°49′37″	120°20′55″	160[c]	fsp vein
GH-14	CJ-25VB	35°49′37″	120°20′55″	160[c]	fsp vein
GH-15	DR-139	NR	NR	160[c]	anorth gabbro
GH-16	DR-1062	NR	NR	160[c]	hbd qtz gabbro
			Logan Quarry (LQ)		
LQ-1	CJ-IUF	NR	NR	160[c]	hbd gabbro
LQ-2	CJ-2	36°52′51″	121°35′15″	160[c]	hbd qtz gabbro
LQ-3	CJ-LQ-1	NR	NR	160[c]	hbd qtz gabbro
LQ-4	CJ-IF	NR	NR	160[c]	hbd qtz gabbro
LQ-5	CJ-3	NR	NR	160[c]	hbd qtz gabbro
LQ-6	SH-6	NR	NR	160[c]	hbd qtz gabbro
LQ-7	SJB-1	NR	NR	160[c]	hbd qtz gabbro
LQ-8	RS92CH1	36°53′57″	121°36′47″	158 ± 2	hbd qtz gabbro
LQ-9	RS92SJ1	36°51′38″	121°33′23″	160[c]	hbd gabbro
LQ-10	DR-588A	NR	NR	160[c]	hbd qtz gabbro

[a]Texture is medium-grained equigranular unless otherwise noted. Varietal minerals listed in order of increasing abundance. Abbreviations are ol, olivine; cpx, clinopyroxene; hbd, hornblende; qtz, quartz; fsp, feldspar; NR, not recorded.

[b]This is intruded by and therefore older than ERP mafic complex; insufficient zircon yield for U/Pb age determination. A 160 Ma age of ERP-GH-LQ mafic terrane is assumed for calculating initial isotope ratios.

[c]This is interpreted age for ERP-GH-LQ mafic complex; there is insufficient zircon yield for U/Pb age determination.

textures of many of these clasts indicate a shallow depth of crystallization, it is possible that some silica was added either by hydrothermal alteration or during weathering and diagenesis. However, on a plot of silica versus total alkalis (Figure 5), it can be seen that total alkali contents are similar to those of other high-silica granites from the California batholiths, suggesting little alkali mobility. The KCGR clasts have relatively high K_2O contents (3.0–5.5 wt %) that are more common in igneous rocks that were intruded into the eastern (continental) side of the mid-Cretaceous batholiths of California [e.g., *Dodge et al.*, 1970].

[12] The JOGD clasts span a wide compositional range and have geochemical characteristics that are similar to those of a primitive oceanic arc (Table 3). The most mafic clasts have <50 wt % SiO_2, contain no modal quartz, and commonly have cumulate textures. More evolved JOGD clasts have intermediate silica contents (55–65 wt % SiO_2) and sparse to abundant modal quartz. The oceanic nature of the JOGD clasts is well illustrated by FeO^*/MgO-TiO_2 variations (Figure 6), where lack of enrichment in TiO_2 with increasing FeO^*/MgO ratio is characteristic of many volcanic arcs [e.g., *Miyashiro*, 1973]. Only one JOGD clast has TiO_2 in excess of

Table 2. Gualala Formation Conglomerate Clast and ERP-GH-LQ Mafic Basement Terrane U/Pb Zircon Isotopic Age Data

Sample	Field Sample	Properties[a]	Fractions[b]	Amount Analyzed, mg	U, ppm	Pb*,[c] ppm	Common Pb, ppm	206Pb/204Pb	206Pb*/238U	%err	207Pb*/235U	%err	207Pb*/206Pb	%err	Error, %	206Pb*/238U	207Pb*/235U	207Pb*/206Pb	6/8-7/5 Correlation Coefficient
											Atomic Ratios[d]					Ages, Ma			
Jurassic Oceanic Gabbro and Diorite Clasts (JOGD): Shell Beach																			
JOGD-5	RS92SP2	hbd qtz gabbro																	
a			D 64–100	1.98	114.0	2.517	0.047	1930	0.022609	0.19	0.15222	0.69	0.048832	0.66		144.1	143.9	139.8	0.2864
b			N 100–150	2.25	117.0	2.606	0.037	2969	0.022691	0.47	0.15311	0.58	0.048936	0.33		144.6	144.6	144.8	0.8158
JOGD-8	RS92SP16	hbd qtz cpx gabbro																	
a			N 64–100	1.95	99.17	2.152	0.461	305.3	0.022292	0.23	0.15521	0.98	0.050499	0.91		142.1	146.5	218.0	0.3896
b			N 150	6.12	199.7	4.312	0.070	2883	0.022148	0.26	0.14982	0.37	0.049060	0.27		141.2	141.8	150.7	0.6913
c			N 150	3.57	214.9	4.469	0.077	3505	0.021871	0.35	0.14912	0.35	0.049450	0.07		139.5	141.1	169.2	0.9811
d			D 150	2.77	201.9	4.347	0.060	4104	0.022668	0.49	0.15416	0.49	0.049326	0.06		144.5	145.6	163.4	0.9925
JOGD-9	RS92SP26	hbd qtz cpx gabbro																	
a			N < 100	1.51	221.4	5.729	0.030	7630	0.029040	0.19	0.16898	0.22	0.049213	0.12		158.6	158.5	158.0	0.8533
Jurassic Oceanic Gabbro and Diorite Clasts (JOGD): Sea Ranch Stable																			
JOGD-14	RS92SP30	hbd qtz gabbro																	
a			D 64–100	2.37	292.6	6.136	0.059	5161	0.022055	0.75	0.15175	0.77	0.049904	0.19		140.6	143.5	190.5	0.9708
b			M1 100–150	2.78	371.9	8.212	0.162	3102	0.022658	0.77	0.15243	0.78	0.048791	0.16		144.4	144.1	137.8	0.9804
c			N 100–150	2.18	214.7	4.712	0.093	2884	0.022528	0.60	0.15186	0.61	0.048891	0.11		143.6	143.6	142.6	0.9840
Cretaceous Continental Granite and Rhyolite Clasts (KCGR): Shell Beach																			
KCGR-1	RS92SP15	hbd biot granodiorite																	
a			N < 64	1.40	884.3	13.457	0.054	6054	0.015188	0.20	0.12072	0.34	0.057651	0.27		97.2	115.7	516.5	0.6187
b			D < 64	0.85	790.4	11.719	4.94	165.0	0.014825	0.25	0.10945	1.24	0.053546	1.18		94.9	105.5	352.0	0.3358
c			N < 64	1.91	943.4	14.540	0.085	8080	0.015438	0.19	0.12144	0.22	0.057049	0.09		98.8	116.4	493.4	0.9094
d			N 64–100	3.48	930.0	16.089	0.290	3424	0.017300	0.20	0.15114	0.23	0.063365	0.11		110.6	142.9	720.5	0.8894
Cretaceous Continental Granite and Rhyolite Clasts (KCGR): Sea Ranch Stable																			
KCGR-4	RS92SP40	hbd biot granite																	
a			N < 64	0.83	961.3	14.848	0.068	2582	0.015795	0.20	0.10626	0.93	0.048791	0.90		101.0	102.5	137.8	0.2583
b			N 64–100	1.87	1205	18.596	0.060	9479	0.015861	0.22	0.10604	0.32	0.048487	0.23		101.4	102.3	123.1	0.6961
c			D 64–100	1.08	898.1	14.592	0.011	3450	0.016611	0.21	0.11596	0.79	0.050631	0.75		106.2	111.4	224.1	0.2986
d			N 100–150	2.32	1283	19.391	0.057	18276	0.015590	0.23	0.10419	0.24	0.048469	0.06		99.7	100.6	122.2	0.9719
Cretaceous Continental Granite and Rhyolite Clasts (KCGR): Smuggler's Cove																			
KCGR-7	RS92SP45	biot granite																	
a			N 64–100	0.42	606.2	9.565	0.533	1054	0.015949	0.28	0.10983	0.32	0.049944	0.15		102.0	105.8	192.4	0.8923
b			N < 64	0.69	976.2	15.459	0.261	3336	0.016013	0.21	0.10858	0.23	0.049178	0.09		102.4	104.7	156.3	0.9199
KCGR-8	RS92SP54	rhyolite																	
a			M2 64–100	1.09	566.7	11.668	1.24	610	0.020168	0.35	0.16874	0.38	0.060680	0.13		128.7	158.3	627.9	0.9386
Cretaceous Continental Granite and Rhyolite Clasts (KCGR): Black Point																			
KCGR-9	RS92SP6	porphyritic biot granite																	
a			D 64–100	0.75	176.9	3.561	4.767	65.88	0.019911	0.30	0.13788	0.89	0.050222	0.80		127.1	131.2	205.3	0.4481
b			N < 64	2.05	835.4	16.095	0.124	7335	0.019014	0.16	0.12871	0.17	0.049093	0.06		121.4	122.9	152.3	0.9442
c			N 100–150	0.5	726.0	13.893	0.653	1264	0.019100	0.21	0.12813	0.25	0.048651	0.14		122.0	122.4	131.1	0.8480
d			N 100–150 AB	0.31	322.7	6.332	0.599	600.7	0.019603	0.48	0.13025	0.54	0.048188	0.25		125.1	124.3	108.5	0.8880
e			N < 64	1.07	939.4	18.418	0.080	10764	0.019320	5.52	0.13103	5.52	0.049189	0.21		123.4	125.0	156.8	0.9992
KCGR-11	RS92SP8	porphyritic biot granite																	
a			M2 64–100	2.37	612.6	9.650	1.408	455.0	0.015664	0.17	0.10774	0.63	0.049885	0.57		100.2	103.9	189.6	0.4661
b			N 64–100	1.5	335.5	5.643	0.835	442.0	0.016681	0.63	0.12164	0.65	0.052888	0.14		106.6	116.6	324.0	0.9765

Table 2. (continued)

Sample	Field Sample	Properties[a]	Fractions[b]	Amount Analyzed, mg	Concentrations U, ppm	Pb*,[c] ppm	Common Pb, ppm	206Pb/204Pb	Atomic Ratios[d] 206Pb*/238U	%err	207Pb*/235U	%err	207Pb*/206Pb	Error, %	Ages, Ma 206Pb*/238U	207Pb*/235U	207Pb*/206Pb	6/8-7/5 Correlation Coefficient
c	KCGR-13 RS92SP55	coarse-grained, equigranular biot granite	N 100–150	0.1	325.1	5.626	0.478	479.0	0.017210	1.58	0.12225	1.69	0.051518	0.58	110.0	117.1	264.1	0.9387
d			N 100–150 AB	0.14	633.5	13.733	0.429	1370	0.021418	0.52	0.17264	0.55	0.058459	0.18	136.6	161.7	547.0	0.9459
a	KCGR-14 RS92SP56	coarse-grained, equigranular biot granite	M2 64–100	0.56	1366	19.361	0.661	1799	0.014388	0.20	0.09543	0.23	0.048106	0.11	92.1	92.6	104.5	0.8874
b			N 64–100	0.62	1041	15.685	0.425	2185	0.015247	0.21	0.10173	0.22	0.048393	0.08	97.5	98.4	118.5	0.9352
a	KCGR-15 RS92SP58	coarse-grained, equigranular biot granite	N 64–100	0.18	1749	27.732	0.455	2865	0.015717	0.27	0.10447	0.32	0.048208	0.16	100.5	100.9	109.5	0.8587
a		porphyritic biot granite	N < 100	3.06	756.1	12.809	1.608	528.1	0.016760	0.18	0.11232	0.22	0.048604	0.13	107.1	108.1	128.8	0.8187
b			N > 100	1.40	701.5	12.345	0.555	1360	0.017524	0.28	0.12401	0.46	0.051326	0.35	112.0	118.7	255.5	0.6519
a	KCGR-17 RS92SP62	porphyritic biot granite	N > 100	2.67	623.2	9.394	0.306	1915	0.014895	0.19	0.09870	0.26	0.048071	0.18	95.3	95.6	102.7	0.7396
a	KCGR-18 RS92SP70	coarse-grained, equigranular biot granite	N < 64	5.12	1305	19.603	0.463	2738	0.015326	0.38	0.10276	0.41	0.048632	0.15	98.0	99.3	130.1	0.9297
b			N 64–100	4.36	1239	16.551	0.516	2080	0.013636	0.60	0.09026	0.63	0.048009	0.17	87.3	87.7	99.7	0.9645
Jurassic Mafic Basement Terrane (ERP-GH-LQ): Eagle Rest Peak (ERP)																		
a	ERP-11 RS92ERP15	hbd qtz gabbro	D > 150	2.84	169.5	4.327	0.041	4777	0.025040	0.23	0.17050	0.29	0.049384	0.18	159.4	159.9	166.1	0.7909
b			N > 150	6.36	208.3	5.297	0.036	7781	0.024784	0.29	0.16832	0.31	0.049257	0.11	157.8	158.0	160.1	0.9373
c			N > 150 AB	3.15	343.9	8.427	0.266	1351	0.023769	0.47	0.16211	0.50	0.049464	0.17	151.4	152.5	169.9	0.9418
a	ERP-14 RS92SC7	hbd tonalite	N 100–150	1.86	215.1	5.18	0.012	8810	0.024656	0.19	0.16835	0.34	0.049519	0.27	157.0	158.0	172.5	0.5891
Jurassic Mafic Basement Terrane (ERP-GH-LQ): Gold Hill (GH)																		
a	GH-11 RS92CV6	hbd qtz gabbro	N > 100	0.84	499.9	12.496	0.061	8231	0.025085	0.28	0.17036	0.33	0.049256	0.19	159.7	159.7	160.0	0.8309
Jurassic Mafic Basement Terrane (ERP-GH-LQ): Logan Quarry (LQ)																		
a	LQ-8 RS92CH1	hbd qtz gabbro	D 100–150	2.75	114.8	2.727	0.024	4307	0.024600	0.19	0.16309	0.84	0.048085	0.78	156.7	153.4	103.4	0.4184
b			N > 150	7.01	71.09	1.685	0.043	2365	0.024724	0.20	0.16829	0.24	0.049368	0.13	157.4	157.9	165.3	0.8431
c			N > 150 AB	6.75	67.36	1.630	0.087	961.6	0.025079	0.24	0.16888	0.77	0.048840	0.73	159.7	158.4	140.1	0.3231

[a]Abbreviations are are biot, biotite; cpx, clinopyroxene; hbd, hornblende; qtz, quartz.

[b]Zircon fractions separated by size and magnetic properties. All magnetic separations performed on a Frantz Magnetic Barrier Separator, model LB-1, with current of 1.7 A and a forward slope of 17.5°. Magnetic fractions as follows: D, diamagnetic; N, nonmagnetic at 2° side slope (weakly paramagnetic); M number is paramagnetic at number of degrees of side slope. Size fraction cuts at 64, 100, and 150 μm. Dissolution and chemical separation techniques modified from *Krogh* [1973]. Data reduction and error analysis based on *Ludwig* [1989]. Decay constants used for age calculation are $\lambda^{238}U = 1.55125 \times 10^{-10}$ yr^{-1} and $\lambda^{235}U = 9.8485 \times 10^{-10}$ yr^{-1} [*Steiger and Jäger*, 1977].

[c]Radiogenic; nonradiogenic correction based on measured Pb blanks of 20 to 380 pgr (30 pg average) (1:19.00:15.35:37.62) and initial Pb from feldspar or from *Stacey and Kramers* [1975] model.

[d]Corrected for mass fractionation of 0.1% per amu for Pb analyses and 0.12% per amu for U analyses based on replicate analyses of NBS-981, NBS-982, NBS-983, and U500 standards.

Table 3a. Gualala Formation Conglomerate Clasts and Jurassic Mafic Basement Terrane (ERP-GH-LQ) Major Element Chemistry[a]

Sample	Field Sample	SiO$_2$	Al$_2$O$_3$	Fe$_2$O$_3$*	MgO	CaO	Na$_2$O	K$_2$O	TiO$_2$	P$_2$O$_5$	MnO	LOI	Total
					Jurassic Oceanic Gabbro and Diorite Clasts (JOGD)								
JOGD-1	CJ-826-1A	55.2	15.36	8.91	5.43	7.54	3.92	0.14	1.18	0.15	0.13	1.31	99.27
JOGD-2	CJ-826-1C	48.9	20.13	7.87	5.51	12.30	2.52	0.19	0.70	0.05	0.13	1.10	99.40
JOGD-3	RS92GU5												
JOGD-4	RS96GU2												
JOGD-5	RS92SP2	60.13	16.67	6.22	2.86	6.63	3.49	0.40	0.55	0.12	0.14	1.82	99.03
JOGD-6	RS92SP13	75.46	13.26	0.74	0.22	2.02	3.97	2.29	0.08	0.02	0.03	0.97	99.06
JOGD-7	RS92SP14	47.21	19.94	5.04	9.50	14.29	1.73	0.07	0.17	0.01	0.08	1.37	99.41
JOGD-8	RS92SP16	57.18	15.85	7.27	4.42	7.16	3.59	0.93	0.52	0.09	0.21	1.64	98.86
JOGD-9	RS92SP26	53.14	16.58	10.06	5.53	8.88	2.12	0.36	0.48	0.04	0.18	2.44	99.81
JOGD-10	CJ-829-2A	47.6	20.70	4.73	8.37	14.83	1.80	0.20	0.16	0.01	0.08	1.47	99.95
JOGD-11	CJ-829-2D	58.12	16.58	8.12	3.34	6.89	3.05	1.19	0.53	0.12	0.14	2.30	100.38
JOGD-12	CJ-829-3A	47.02	17.67	5.49	10.75	14.68	1.53	0.12	0.21	0.01	0.09	1.27	98.84
JOGD-13	RS92SP27	58.09	17.87	6.19	3.34	7.90	2.53	0.26	0.34	0.06	0.14	2.75	99.47
JOGD-14	RS92SP30	60.72	17.23	5.50	2.74	6.32	3.32	0.86	0.35	0.10	0.11	1.87	99.12
JOGD-15	RS92SP31	47.63	19.56	6.10	7.76	14.44	1.90	0.20	0.42	0.04	0.10	1.40	99.55
JOGD-16	RS92SP32	62.66	16.11	5.90	2.28	6.15	2.71	1.00	0.27	0.09	0.14	2.10	99.41
					Cretaceous Continental Granite and Rhyolite Clasts (KCGR)								
KCGR-1	RS92SP15	68.09	15.46	3.10	1.05	2.81	3.97	3.04	0.51	0.13	0.04	0.83	99.03
KCGR-2	CJ-829-3A												
KCGR-3	CJ-829-4B	70.39	12.74	2.08	0.48	3.85	3.57	3.35	0.24	0.05	0.05	2.30	99.10
KCGR-4	RS92SP40	73.89	13.22	1.44	0.41	2.12	3.62	3.79	0.19	0.04	0.03	1.16	99.91
KCGR-5	RS92SP42	74.73	13.38	1.51	0.40	0.73	4.16	3.49	0.23	0.05	0.03	0.85	99.56
KCGR-6	RS92SP43	76.81	12.53	0.50	0.11	0.35	4.09	4.11	0.04	0.01	0.02	0.45	99.02
KCGR-7	RS92SP45	74.73	13.22	1.81	0.26	0.68	4.20	3.80	0.14	0.03	0.03	1.55	100.45
KCGR-8	RS92SP54	75.47	13.24	1.80	0.40	<0.01	3.92	3.57	0.26	0.04	0.03	1.03	99.76
KCGR-9	RS92SP6	76.58	12.80	1.46	0.20	0.87	3.23	3.80	0.15	0.02	0.02	0.56	99.69
KCGR-10	RS92SP7	77.94	12.13	0.88	0.12	0.39	3.04	5.31	0.06	0.01	0.01	0.33	100.22
KCGR-11	RS92SP8	76.61	12.57	1.52	0.19	0.34	3.28	4.22	0.15	0.01	0.01	0.72	99.62
KCGR-12	RS92SP10	72.44	14.19	2.50	1.03	0.78	3.64	3.57	0.48	0.10	0.08	1.36	100.17
KCGR-13	RS92SP55	78.61	11.91	0.76	0.16	0.30	4.23	3.79	0.07	0.02	0.01	0.40	100.26
KCGR-14	RS92SP56	78.16	12.09	0.84	0.12	0.10	3.95	3.72	0.09	0.00	0.00	0.54	99.61
KCGR-15	RS92SP58	78.01	11.74	1.07	0.24	0.07	2.96	4.66	0.13	0.02	0.02	0.74	99.66
KCGR-16	RS92SP60	79.70	11.67	1.09	0.13	0.08	3.73	3.42	0.09	0.00	0.01	0.45	100.37
KCGR-17	RS92SP62	76.62	11.88	1.47	0.44	0.21	3.72	4.66	0.22	0.04	0.02	0.73	100.00
KCGR-18	RS92SP70	78.42	11.65	1.16	0.12	0.29	3.84	4.31	0.08	0.02	0.02	0.50	100.40
					Eagle Rest Peak (ERP)								
ERP-1	RS92ER1	49.03	14.99	10.63	7.48	12.32	2.30	0.18	1.45	0.10	0.16	0.87	99.51
ERP-2	CJ-40A	50.64	10.19	5.70	15.59	15.43	0.79	0.11	0.12	0.00	0.14	0.91	99.62
ERP-3	CJ-41A	49.88	14.37	2.54	10.70	21.12	0.64	0.04	0.30	0.01	0.03	0.51	100.14
ERP-4	CJ-41A-A	47.28	17.17	6.41	10.85	14.03	1.14	0.28	0.24	0.01	0.09	1.48	98.98
ERP-5	CJ-42A	48.18	17.17	5.29	10.92	15.45	1.46	0.04	0.21	0.01	0.09	1.69	100.51
ERP-6	CJ-42B												
ERP-7	CJ-43A	69.45	14.00	3.36	0.84	2.34	4.25	3.02	0.34	0.07	0.06	1.91	99.64
ERP-8	CJ-43C	56.16	14.59	6.55	6.99	9.99	2.48	0.59	0.40	0.09	0.15	1.14	99.13
ERP-9	RS92ER2	44.4	21.32	4.74	9.86	15.98	0.48	0.03	0.05	0.01	0.08	1.59	98.54
ERP-10	RS92ER9	49.7	17.26	4.83	8.55	14.77	2.31	0.10	0.30	0.01	0.09	1.69	99.61
ERP-11	RS92ER15	55.07	16.45	6.78	6.35	9.52	2.53	0.23	0.35	0.03	0.12	1.35	98.78
ERP-12	RS92ER18	52.83	1.91	8.56	23.70	12.56	0.61	0.05	0.09	<0.01	0.22	0.45	100.98
ERP-13	RS92ER28	47.63	18.01	5.34	10.40	14.83	1.53	0.06	0.21	0.01	0.09	1.56	99.67
ERP-14	RS92SC1	63.9	15.79	6.01	2.03	5.79	2.78	0.65	0.30	0.05	0.13	1.39	98.82
ERP-15	RS92SC7	63.1	16.06	6.38	2.14	6.10	2.82	0.68	0.33	0.06	0.13	1.33	99.13
ERP-16	CJ-40B												
ERP-17	CJ-42BQ												
					Gold Hill (GH)								
GH-1	CJ-21												
GH-2	CJ-22												
GH-3	CJ-24	52.31	14.32	11.90	7.39	10.57	1.39	0.22	0.58	0.08	0.19	0.74	99.69
GH-4	CJ-25												
GH-5	CJ-27												
GH-6	CJ-28												
GH-7	CJ-29												
GH-8	SH-4	51.65	17.85	9.58	5.95	11.10	1.49	0.17	0.31	0.03	0.16	0.36	98.65
GH-9	CJ-GH-1												
GH-10	RS92CV5	52.29	15.45	11.31	6.36	9.84	1.47	0.22	0.58	0.15	0.19	2.46	100.32
GH-11	RS92CV6	52.25	14.73	11.49	6.91	9.98	1.25	0.20	0.56	0.05	0.21	2.36	99.99
GH-12	CJ-24V												
GH-13	CJ-25VA												
GH-14	CJ-25VB												

Table 3a. (continued)

Sample	Field Sample	SiO_2	Al_2O_3	Fe_2O_3*	MgO	CaO	Na_2O	K_2O	TiO_2	P_2O_5	MnO	LOI	Total
					Logan Quarry (LQ)								
LQ-1	CJ-IUF												
LQ-2	CJ-2												
LQ-3	CJ-LQ-1	47.31	24.45	2.83	5.76	15.34	1.81	0.03	0.13	0.01	0.05	1.73	99.45
LQ-4	CJ-IF	52.11	18.17	9.76	4.42	9.89	2.03	0.20	0.61	0.08	0.16	1.32	98.75
LQ-5	CJ-3												
LQ-6	SH-6												
LQ-7	SJB-1												
LQ-8	RS92CH1	56.57	18.35	7.38	3.01	7.88	2.90	0.57	0.53	0.08	0.13	1.94	99.34
LQ-9	RS92SJ1	48.37	15.25	7.70	10.37	13.29	1.79	0.07	0.66	<0.01	0.12	1.11	98.73

[a] Major element oxides in weight percent. LOI, loss on ignition. All Fe is Fe_2O_3.

1 wt %, which plots in the low-Ti end of the Franciscan mid-ocean ridge basalt (MORB) field [*Shervais*, 1990].

[13] The KCGR clasts are uniformly enriched in light rare earth elements (LREE; $Ce_N \sim 50–120$ times chondritic) relative to heavy rare earth elements (HREE; $Yb_N \sim 5–30$ times chondritic), and have pronounced negative Eu anomalies (Figure 7a). These patterns are typical of granites in the southern Sierra Nevada and central Salinian block [*Ross*, 1982, 1989]. A single exception is the REE pattern for clast KCGR-6, which has high total REE concentrations ($\sim 30–40$ times chondritic) but a relatively low LREE/HREE ratio, possibly indicative of fractionation of LREE-enriched accessory minerals [*Miller and Mittlefehldt*, 1982].

[14] The REE patterns of the JOGD clasts can be subdivided into three subgroups (Figure 7b). The most mafic clasts, which have no modal quartz and display cumulate textures, have low LREE/HREE ratios, low overall REE concentrations, and moderate to strongly positive Eu anomalies. These samples likely reflect plagioclase accumulation. The majority of JOGD clasts have relatively flat REE patterns ($\sim 6–11$ times chondritic) and little or no Eu anomaly. Finally, four of the more silicic JOGD clasts have somewhat more fractionated REE patterns that are characterized by high LREE/HREE ratios and small to moderate negative Eu anomalies.

3.1.3. Isotopic Compositions

[15] Oxygen isotope ratios of the KCGR clasts ($\delta^{18}O_{magma} = +8.2$ to $+11.2‰$, as inferred from analyses of quartz separates; Table 4) are higher than those of the mantle and require a significant component of upper continental crustal material. In the California batholiths, $\delta^{18}O_{magma}$ values greater than $+9‰$ are common only in the eastern Peninsular Ranges, the Salinian block, the western Mojave Desert, and the southeastern SNB [*Taylor and Silver*, 1978; *Masi et al.*, 1981; *Solomon*, 1989; *Solomon and Taylor*, 1989]. Distinctly lower $\delta^{18}O_{magma}$ values of JOGD clasts ($+6.3‰$ to $+9.0‰$) probably reflect mantle-derived magmas that experienced limited interaction with the crust. δD values of two JOGD clasts are relatively high (about $-50‰$), suggesting hydrothermal alteration with ocean water (Figure 8).

[16] Strontium, Nd, and Pb isotope compositions of the KCGR clasts indicate involvement of old continental crust in source bodies (Figure 9). Initial $^{87}Sr/^{86}Sr$ isotope ratios of KCGR clasts are uniformly greater than 0.7060 and most (12 out of 16) clasts have $^{87}Sr/^{86}Sr_{init}$ between 0.7075 and 0.7090 (Table 4). These are relatively radiogenic Sr isotope compositions for the Cretaceous batholiths of California, and such compositions are diagnostic of the central or eastern regions of the arc [*Kistler and Peterman*, 1973, 1978; *Kistler and*

Ross, 1990; *Mattinson*, 1990]. The $\varepsilon_{Nd}(t)$ values range from $+1$ to -7, also indicating involvement of old continental crust, and are most similar to those of the central and eastern parts of the California batholiths [*DePaolo*, 1981; *Mattinson*, 1990]. Sr-Nd isotope variations of the bulk of the KCGR clasts diverge significantly from the tight trend characteristic of Cretaceous Cordilleran granitoids (Figure 9c), a feature that seems to be restricted to the Mojave-Salinia segment of the arc [*Schott and Johnson*, 1998a]. Lead isotope variations (Figure 10 and Table 4) of KCGR clasts follow the trend established by other Cretaceous granitoids in the California batholiths [*Mattinson*, 1990; *Chen and Tilton*, 1991]. The KCGR clasts have moderately high $^{207}Pb/^{204}Pb$ ratios (Figure 10), similar to those seen in the Salinian block and western Mojave [*Wooden et al.*, 1988; *Mattinson*, 1990] but not at all similar to the extremely high $^{207}Pb/^{204}Pb$ ratios that are characteristic of the eastern Mojave Desert [*Wooden et al.*, 1988].

[17] Measured radiogenic and stable isotope compositions indicate that the sources of the JOGD clasts are much more primitive than those of the KCGR clasts and/or interacted less with old continental crust. Initial $^{87}Sr/^{86}Sr$ isotope ratios of JOGD clasts are generally between 0.7030 and 0.7040 (Table 4), relatively primitive compositions that are indicative of a depleted-mantle source, although a few are as high as 0.7052; these high ratios seem likely to reflect alteration by seawater [e.g., *McCulloch et al.*, 1981], in concert with their high δD values (Figure 8). The $\varepsilon_{Nd}(t)$ values range from $+5.5$ to $+8.6$ and also indicate a depleted-mantle source. For the most part, Sr and Nd isotope variations (Figure 9c) cluster within the fields of primitive arcs or EMORB [e.g., *Zindler et al.*, 1979; *Hart et al.*, 1986; *Lin et al.*, 1990; *Stern et al.*, 1993]. Lead isotope compositions are more radiogenic than those of modern east Pacific MORB from the Juan de Fuca plate and are more primitive than those of Coast Range Ophiolite samples from the Point Sal Ophiolite, but similar to those of the Josephine Ophiolite [*Chen and Shaw*, 1982] (Figure 10). A relatively steep linear trend in both $^{206}Pb/^{204}Pb$-$^{207}Pb/^{204}Pb$ and $^{206}Pb/^{204}Pb$-$^{208}Pb/^{204}Pb$ variations (Figure 10) in some of the Gualala gabbros may reflect assimilation and mixing with an older Pb component that had a low Th/U ratio [*Church*, 1976; *Woodhead and Fraser*, 1985].

3.2. Mafic Basement Terrane (ERP-LQ-GH)

[18] It is generally accepted that Jurassic gabbroic rocks at Eagle Rest Peak (ERP), Logan Quarry (LQ), and Gold Hill (GH) were derived from the same mafic basement terrane [*Ross et al.*, 1973; *James et al.*, 1993], and the ERP locality probably represents exposures of this terrane that

Table 3b. Gualala Formation Conglomerate Clasts and Jurassic Mafic Basement Terrane (ERP-GH-LQ) Trace Element Chemistry[a]

Sample	Field Sample	Rb	Sr	Y	Zr	Nb	Ba	Sc	V	Cr	Ni	Cu	Zn
					Jurassic Oceanic Gabbro and Diorite Clasts (*JOGD*)								
JOGD-1	CJ-826-1A												
JOGD-2	CJ-826-1C												
JOGD-3	RS92GU5												
JOGD-4	RS96GU2												
JOGD-5	RS92SP2	10	351	23	71	8	138	26	236	15	7	14	76
JOGD-6	RS92SP13	33	206	13	52	2	984	4	7	2	3	<1	10
JOGD-7	RS92SP14	7	158	10	18	5	19	32	85	569	150	69	39
JOGD-8	RS92SP16	20	386	39	65	9	223	39	175	75	17	59	90
JOGD-9	RS92SP26	12	195	20	31	6	145	60	362	59	16	23	89
JOGD-10	CJ-829-2A												
JOGD-11	CJ-829-2D												
JOGD-12	CJ-829-3A												
JOGD-13	RS92SP27	9	311	16	41	5	97	27	208	14	2	7	52
JOGD-14	RS92SP30	23	364	22	107	8	315	18	97	40	16	1	50
JOGD-15	RS92SP31	10	222	15	32	6	71	45	165	86	81	ND	22
JOGD-16	RS92SP32	19	345	17	52	6	313	21	132	11	1	3	41
					Cretaceous Continental Granite and Rhyolite Clasts (*KCGR*)								
KCGR-1	RS92SP15	94	490	13	199	11	940	7	35	8	7	ND	63
KCGR-2	CJ-829-3A												
KCGR-3	CJ-829-4B												
KCGR-4	RS92SP40	97	151	21	139	10	1377	5	10	6	6	ND	28
KCGR-5	RS92SP42	113	196	29	193	13	874	8	7	2	7	ND	38
KCGR-6	RS92SP43	200	13	85	95	25	158	10	ND	2	8	ND	17
KCGR-7	RS92SP45	138	107	22	181	12	894	8	ND	2	7	ND	42
KCGR-8	RS92SP54	103	113	45	191	11	928	9	18	0	1	3	79
KCGR-9	RS92SP6	87	178	15	83	5	653	4	14	4	1	5	16
KCGR-10	RS92SP7	243	86	8	72	ND	95	2	ND	3	6	ND	ND
KCGR-11	RS92SP8	142	132	21	127	8	725	3	9	2	1	5	29
KCGR-12	RS92SP10	123	289	20	178	15	738	8	47	11	7	4	65
KCGR-13	RS92SP55	149	24	12	162	12	470	3	ND	2	8	ND	32
KCGR-14	RS92SP56	126	42	18	170	17	627	3	4	1	1	15	28
KCGR-15	RS92SP58	156	131	9	95	16	502	3	10	8	1	<1	10
KCGR-16	RS92SP60	115	52	35	193	16	667	5	5	3	1	2	28
KCGR-17	RS92SP62	190	161	12	124	<1	669	4	20	7	11	<1	10
KCGR-18	RS92SP70	193	39	8	144	11	480	3	3	2	12	<1	117
					Eagle Rest Peak (*ERP*)								
ERP-1	RS92ER1	2	160	30	89	4	29	52	271	340	89	65	78
ERP-2	CJ-40A												
ERP-3	CJ-41A												
ERP-4	CJ-41A-A												
ERP-5	CJ-42A												
ERP-6	CJ-42B												
ERP-7	CJ-43A												
ERP-8	CJ-43C												
ERP-9	RS92ER2	6	133	8	14	6	ND	29	54	302	73	0	16
ERP-10	RS92ER9	7	180	12	19	5	7	58	153	390	105	59	37
ERP-11	RS92ER15	9	177	25	77	7	90	49	159	11	17	148	71
ERP-12	RS92ER18	1	18	2	<1	1	12	84	175	1900	138	8	47
ERP-13	RS92ER28	7	160	11	18	4	2	45	112	859	184	97	46
ERP-14	RS92SC1	16	141	20	32	7	198	31	123	11	3	1559	373
ERP-15	RS92SC7	15	158	18	39	7	186	30	134	10	3	26	66
ERP-16	CJ-40B												
ERP-17	CJ-42BQ												
					Gold Hill (*GH*)								
GH-1	CJ-21												
GH-2	CJ-22												
GH-3	CJ-24												
GH-4	CJ-25												
GH-5	CJ-27												
GH-6	CJ-28												
GH-7	CJ-29												
GH-8	SH-4												
GH-9	CJ-GH-1												
GH-10	RS92CV5	3	106	13	30	2	35	73	377	219	31	104	82
GH-11	RS92CV6	3	106	11	26	2	19	77	405	235	33	123	87
GH-12	CJ-24V												
GH-13	CJ-25VA												
GH-14	CJ-25VB												

Table 3b. (continued)

Sample	Field Sample	Rb	Sr	Y	Zr	Nb	Ba	Sc	V	Cr	Ni	Cu	Zn
						Logan Quarry (LQ)							
LQ-1	CJ-IUF												
LQ-2	CJ-2												
LQ-3	CJ-LQ-1												
LQ-4	CJ-IF												
LQ-5	CJ-3												
LQ-6	SH-6												
LQ-7	SJB-1												
LQ-8	RS92CH1	12	213	20	39	7	162	30	185	14	3	44	60
LQ-9	RS92SJ1	1	135	16	23	2	<6	72	210	757	203	6	25

Sample	Field Sample	Ce	Nd	Sm	Eu	Gd	Dy	Er	Yb
				Jurassic Oceanic Gabbro and Diorite Clasts (JOGD)					
JOGD-1	CJ-826-1A	12.535	9.950	3.006	1.093	3.759	4.464	2.801	2.623
JOGD-2	CJ-826-1C	5.154	4.158	1.321	0.584	1.714	2.086	1.320	1.242
JOGD-3	RS92GU5	8.172	6.371	2.001	0.721	2.606	3.065	1.936	1.855
JOGD-4	RS96GU2	3.909	3.305	1.139	0.422	1.593	2.066	1.440	1.538
JOGD-5	RS92SP2	12.097	8.584	2.244	0.793	2.634	2.884	1.914	1.977
JOGD-6	RS92SP13	23.061	9.685	1.767	0.438	1.585	1.706	1.220	1.543
JOGD-7	RS92SP14	0.864	0.931	0.362	0.309	0.570	0.686	0.414	0.369
JOGD-8	RS92SP16	20.764	18.110	4.920	1.103	5.090	5.603	3.785	4.178
JOGD-9	RS92SP26	4.807	4.030	1.371	0.536	1.919	2.347	1.598	1.633
JOGD-10	CJ-829-2A	1.037	0.812	0.299	0.286	0.443	0.558	0.282	0.294
JOGD-11	CJ-829-2D	21.851	12.969	2.953	0.778	2.812	2.928	1.854	1.896
JOGD-12	CJ-829-3A								
JOGD-13	RS92SP27	4.834	3.587	1.024	0.501	1.329	1.553	1.090	1.212
JOGD-14	RS92SP30	22.547	11.600	2.490	0.785	2.539	2.597	1.732	1.869
JOGD-15	RS92SP31	3.280	2.805	0.940	0.431	1.345	1.583	1.008	0.928
JOGD-16	RS92SP32	7.298	4.735	1.325	0.467	1.570	1.785	1.277	1.496
				Cretaceous Continental Granite and Rhyolite Clasts (KCGR)					
KCGR-1	RS92SP15	63.868	26.131	4.450	0.938	3.161	2.178	1.047	0.983
KCGR-2	CJ-829-3A	52.143	25.136	5.535	1.197	5.285	5.625	3.524	3.617
KCGR-3	CJ-829-4B	66.767	27.759	4.987	0.820	3.994	3.409	1.873	1.761
KCGR-4	RS92SP40	49.658	21.356	4.104	0.717	3.542	3.263	1.838	1.720
KCGR-5	RS92SP42	57.719	24.645	5.089	0.725	4.409	4.624	2.748	2.892
KCGR-6	RS92SP43	24.469	18.239	7.878	0.273	9.790	14.057	8.563	7.964
KCGR-7	RS92SP45	58.835	25.316	4.938	0.734	3.961	3.957	2.356	2.636
KCGR-8	RS92SP54	61.688	33.110	7.039	1.008	6.608	7.022	4.322	4.221
KCGR-9	RS92SP6	32.566	13.183	2.586	0.435	2.410	2.514	1.669	1.883
KCGR-10	RS92SP7	49.405	13.318	2.128	0.135	1.704	1.645	1.182	1.767
KCGR-11	RS92SP8	48.719	19.444	3.489	0.584	3.077	3.472	2.303	2.438
KCGR-12	RS92SP10	67.741	25.671	4.592	1.067	3.690	3.445	2.066	2.291
KCGR-13	RS92SP55	49.237	18.428	2.897	0.381	2.025	2.031	1.280	1.441
KCGR-14	RS92SP56	58.677	25.770	4.735	0.569	3.561	3.390	2.088	0.941
KCGR-15	RS92SP58	52.664	15.454	2.344	0.293	1.672	1.683	1.101	1.442
KCGR-16	RS92SP60	45.695	21.229	5.023	0.628	5.086	6.139	4.059	4.323
KCGR-17	RS92SP62	53.692	17.716	2.801	0.308	1.986	1.767	1.087	1.289
KCGR-18	RS92SP70	46.306	17.253	3.040	0.498	2.125	1.712	0.964	1.080
				Eagle Rest Peak (ERP)					
ERP-1	RS92ER1	10.387	9.089	3.033	1.168	4.120	4.779	2.947	2.750
ERP-2	CJ-40A	0.558	0.657	0.283	0.187	0.430	0.571	0.367	0.337
ERP-3	CJ-41A	1.339	1.859	0.785	0.466	1.165	1.469	0.879	0.777
ERP-4	CJ-41A-A	1.297	1.337	0.536	0.356	0.809	1.017	0.633	0.551
ERP-5	CJ-42A	0.734	0.978	0.463	0.303	0.732	0.970	0.591	0.530
ERP-6	CJ-42B								
ERP-7	CJ-43A	0.789	0.998	0.445	0.301	0.703	0.912	0.553	0.491
ERP-8	CJ-43C	10.922	6.805	1.764	0.600	1.894	2.005	1.277	1.307
ERP-9	RS92ER2								
ERP-10	RS92ER9								
ERP-11	RS92ER15								
ERP-12	RS92ER18								
ERP-13	RS92ER28								
ERP-14	RS92SC1								
ERP-15	RS92SC7	5.655	3.856	1.137	0.458	1.541	1.922	1.400	1.562
ERP-16	CJ-40B								
ERP-17	CJ-42BQ								
				Gold Hill (GH)					
GH-1	CJ-21								
GH-2	CJ-22								
GH-3	CJ-24	4.888	4.342	1.394	0.479	1.817	2.298	1.559	1.603

Table 3b. (continued)

Sample	Field Sample	Rb	Sr	Y	Zr	Nb	Ba	Sc	V	Cr	Ni	Cu	Zn
GH-4	CJ-25												
GH-5	CJ-27												
GH-6	CJ-28												
GH-7	CJ-29												
GH-8	SH-4	2.771	2.279	0.752	0.386	1.006	1.326	0.923	0.991				
GH-9	CJ-GH-1												
GH-10	RS92CV5												
GH-11	RS92CV6												
GH-12	CJ-24V												
GH-13	CJ-25VA												
GH-14	CJ-25VB												
					Logan Quarry (LQ)								
LQ-1	CJ-IUF												
LQ-2	CJ-2												
LQ-3	CJ-LQ-1	0.679	n.d.	0.346	0.230	0.532	0.471	0.282	0.248				
LQ-4	CJ-IF	4.834	4.911	1.635	0.636	2.190	2.722	1.828	1.774				
LQ-5	CJ-3												
LQ-6	SH-6												
LQ-7	SJB-1												
LQ-8	RS92CH1												
LQ-9	RS92SJ1												

[a]Trace element abundances are in parts per million; ND, not determined. All abundances are determined by XRF, except Rb, Sr, and REE are determined by isotope dilution mass spectrometry.

have not been displaced by Neogene tectonics. U/Pb zircon crystallization ages in all localities are concordant or near concordant at about 158 Ma to 160 Ma (Figure 4b and Table 2). These U/Pb ages are in excellent agreement with previously published ages from these localities by *James et al.* [1993]. Particularly important is the 160 ± 1 Ma concordant zircon fraction from Gold Hill, a locality which had previously yielded a discordant U/Pb zircon age of ~144 Ma [*James et al.*, 1993]. We therefore propose an emplacement age of 160 ± 2 Ma for all three bodies. Chemical and isotopic compositions of ERP-LQ-GH are broadly similar to those of the JOGD suite (Tables 3 and 4). *Reitz* [1986] recognized a boninitic crystallization sequence at ERP, a sequence that is commonly associated with magmatism in a forearc tectonic environment [*Hawkins et al.*, 1984]. An oceanic arc origin is also indicated by the lack of TiO_2 enrichment with increasing FeO*/MgO ratios (Figure 6) [*Reitz*, 1986]. The REE patterns from ERP-LQ-GH are generally flat, although some of the cumulate rocks from Eagle Rest Peak have strongly LREE depleted patterns, and one quartz-bearing gabbro has a weakly LREE-enriched pattern (Figure 7c); in general, however, these patterns overlap those of the JOGD clasts. Whole rock $\delta^{18}O$ and δD values of the ERP-LQ-GH rocks (Figure 8 and Table 4) scatter from primary igneous compositions; the relatively high δD values most likely reflect hydrothermal alteration by seawater, similar to the JOGD clasts. Rocks from ERP-LQ-GH have initial $^{87}Sr/^{86}Sr$ ratios that are mostly in the range of 0.7025 to 0.7035, and are therefore slightly more primitive than most of the JOGD suite, although some overlap occurs (Figure 9). The $\varepsilon_{Nd}(t)$ value ranges from +5.1 to +8.7, in close agreement with values observed for the JOGD clasts (Figure 9).

4. Discussion

[19] Provenance characteristics of Gualala Formation conglomerates, taken in their depositional context, provide

relatively distinctive constraints on sediment sources. The data provide general constraints on source terranes, rather than identifying locally restrictive sources, such as those required to establish piercing points across the San Andreas fault system [*Cowan et al.*, 1997]. Nevertheless, provenance constraints have important implications for Late Cretaceous tectonics and paleolatitudes of the coastal components of the western Cordillera.

4.1. Provenance Constraints: Juxtaposed Oceanic and Continental Sources in a Near-Forearc Setting

[20] The presence of cobble- and boulder-sized conglomerate clasts of markedly different compositions within the same beds in the Gualala Formation requires that the terranes from which these two distinct rock types were derived were juxtaposed adjacent to the basin during the latest Cretaceous. In the Cordilleran batholiths of western North America, rocks of these contrasting types are not known to occur in close proximity to each other; rather, they are most often separated by a wide expanse of rocks of intermediate compositions (i.e., tonalite and granodiorite) that have a continuous gradation in isotopic compositions [e.g., *Kistler and Peterman*, 1973, 1978; *Taylor and Silver*, 1978; *DePaolo*, 1981; *Chen and Tilton*, 1991; *Bateman*, 1992]. Although there are minor to significant isotopic steps in some regions, such as the central Peninsular Ranges batholith [*Silver et al.*, 1979] or the western Idaho batholith [*Fleck and Criss*, 1985], granites and rhyolites of continental affinity are not found in close proximity to the forearc in any of the California batholiths when viewed in the configuration of their magmatic emplacement.

[21] Of the exposed possible source terranes, it seems most likely that the Gualala Formation conglomerates were derived from the Gabilan-San Emigdio Ranges region that would have been a contiguous source terrane in the Late Cretaceous (Figure 11). In the San Emigdio Mountains of the southern Sierran tail, granitic rocks of

Table 4. Gualala Formation Conglomerate Clasts and Jurassic Mafic Basement Terrane (ERP-GH-LQ) Isotope Data[a]

Sample	Field Sample	Age, Ma	Rb, ppm	Sr, ppm	$\frac{^{87}Rb}{^{86}Sr}$	$\frac{^{87}Sr}{^{86}Sr}$ Measured	$\frac{^{87}Sr}{^{86}Sr}$ Initial	Sm, ppm	Nd, ppm	$\frac{^{147}Sm}{^{144}Nd}$	$\frac{^{143}Nd}{^{144}Nd}$ Measured	$\varepsilon_{Nd}(t)$	$\frac{^{206}Pb}{^{204}Pb}$	$\frac{^{207}Pb}{^{204}Pb}$	$\frac{^{208}Pb}{^{204}Pb}$	$\delta^{18}O$ Quartz	$\delta^{18}O$ Magma	$\delta^{18}O$ WR	δD WR
Jurassic Oceanic Gabbros and Quartz Diorites (JOGD)																			
JOGD-1	CJ-826-1A	150	2.394	200.5	0.0345	0.703814	0.70374	3.006	9.950	0.1824	0.513058	8.47							
JOGD-2	CJ-826-1C	150	2.845	215.1	0.0383	0.703081	0.70300	1.321	4.179	0.1909	0.513050	8.15							
JOGD-3	RS92GU5	150						1.995	6.332	0.1903	0.513071	8.58							
JOGD-4	RS96GU2	150						1.135	3.285	0.2087	0.513073	8.25							
JOGD-5	RS92SP2	145	6.517	343.6	0.0549	0.7033918	0.70328	2.244	8.555	0.1584	0.513012	8.00	18.292	15.520	38.825	9.0	7.5		
JOGD-6	RS92SP13	150	33.000	206.0	0.4315			1.761	9.626	0.1105	0.512978	8.28	18.544	15.620	38.285	8.3	6.8		
JOGD-7	RS92SP14	150	1.930	148.5	0.0376	0.7034647	0.70338	0.362	0.913	0.2393	0.512961	5.49							
JOGD-8	RS92SP16	145	18.179	371.6	0.1415	0.7036771	0.70339	4.922	18.072	0.1645	0.512989	7.44	18.472	15.589	38.133	8.9	7.4		
JOGD-9	RS92SP26	158.5	7.661	193.4	0.1146	0.7045792	0.70432	1.366	4.004	0.2060	0.512981	6.50	18.264	15.563	37.927	8.4	6.9		
JOGD-10	CJ-829-2A	150	9.347	179.3	0.1508	0.705493	0.70517												
JOGD-11	CJ-829-2D	150	30.549	480.1	0.1841	0.703959	0.70357	2.953	13.195	0.1351	0.512926	6.80							
JOGD-12	CJ-829-3A	150																	
JOGD-13	RS92SP27	150	4.746	296.6	0.0463	0.7037787	0.70368	1.020	3.564	0.1728	0.512989	7.30	18.287	15.608	38.006	8.5	7.0		
JOGD-14	RS92SP30	144	21.751	341.2	0.1844	0.7039991	0.70362	2.491	11.570	0.1300	0.512888	6.10							
JOGD-15	RS92SP31	150	6.748	214.6	0.0910	0.7039415	0.70375	0.941	2.784	0.2040	0.513051	7.93							
JOGD-16	RS92SP32	150	18.543	341.6	0.1570	0.7039699	0.70364	1.330	4.706	0.1707	0.512953	6.65	18.189	15.387	37.299	10.5	9.0		
JOGD-17	ABc-1	150	17	125	0.3935	0.70465	0.70381											6.6	−47
JOGD-18	SR-3	150	20	153	0.3782	0.70458	0.70377											6.3	−53
Cretaceous Continental Granitic & Rhyolitic Clasts (KCGR)																			
KCGR-1	RS92SP15	85	99.906	481.6	0.6005	0.7085639	0.70784	4.437	25.973	0.1031	0.512240	−6.75	19.549	15.801	39.196	12.4	10.9		
KCGR-2	CJ-829-3A	100	97.158	204.2	1.3774	0.709979	0.70802	5.520	24.983	0.1334	0.512388	−4.07							
KCGR-3	CJ-829-4B	100	88.291	210.9	1.2117	0.707975	0.70625	4.972	27.591	0.1088	0.512528	−1.02							
KCGR-4	RS92SP40	101	108.278	146.5	2.1389	0.7091769	0.70611	4.105	21.315	0.1163	0.512520	−1.27	19.005	15.655	38.690	12.5	11.0		
KCGR-5	RS92SP42	100	112.819	191.3	1.7075	0.7107051	0.70828	5.075	24.496	0.1251	0.512366	−4.40	19.514	15.795	39.183	12.5	11.0		
KCGR-6	RS92SP43	100	200.000	13.0	41.4442			7.857	18.128	0.2617	0.512429	−4.91	19.406	15.759	38.995	12.3	10.8		
KCGR-7	RS92SP45	101	120.640	102.3	3.4165	0.7134254	0.70852	4.940	25.270	0.1180	0.512388	−3.87	19.428	15.776	39.074	11.1	9.6		
KCGR-8	RS92SP54	100	105.044	104.6	2.9077	0.7110146	0.70688	7.018	32.909	0.1288	0.512405	−3.69	19.764	15.791	39.413	11.4	9.9		
KCGR-9	RS92SP6	125	85.166	177.6	1.3883	0.709005	0.70654	2.587	13.151	0.1187	0.512643	1.33	18.906	15.701	38.769	10.5	9.0		
KCGR-10	RS92SP7	100	241.663	80.2	8.7297	0.7202991	0.70789	2.120	13.237	0.0967	0.512396	−3.45	19.303	15.733	38.939	11.4	9.9		
KCGR-11	RS92SP8	100	145.791	128.7	3.2791	0.7130564	0.70840	3.490	19.405	0.1086	0.512242	−6.61	19.453	15.728	38.996	9.9	8.4		
KCGR-12	RS92SP10	100	123.000	289.0	1.1465			4.578	25.515	0.1083	0.512388	−3.54	19.361	15.744	39.075	12.6	11.1		
KCGR-13	RS92SP55	97	143.515	21.9	19.0032	0.7334738	0.70728	2.899	18.390	0.0952	0.512421	−3.62	19.418	15.742	39.037	12.6	11.1		
KCGR-14	RS92SP56	100	124.534	39.0	9.2653	0.7221306	0.70896	4.721	25.614	0.1113	0.512432	−3.15	19.395	15.776	39.171	10.8	9.3		
KCGR-15	RS92SP58	106	160.086	128.1	3.6198	0.7133311	0.70788	2.336	15.360	0.0918	0.512458	−2.59	19.606	15.793	39.361	10.7	9.2		
KCGR-16	RS92SP60	100	108.417	48.5	6.4787	0.717482	0.70828	5.008	21.100	0.1433	0.512361	−2.83	19.501	15.803	39.185	12.7	11.2		
KCGR-17	RS92SP62	95	172.848	155.6	3.2175	0.7127644	0.70842	2.792	17.608	0.0957	0.512458	−4.18	19.267	15.686	38.821	9.7	8.2		
KCGR-18	RS92SP70	98	187.074	36.5	14.8856	0.7298199	0.70909	2.939	16.632	0.1067	0.512404	−3.44	19.321	15.693	38.897				
Eagle Rest Peak (ERP) - Gold Hill (GH) - Logan Quarry (LQ) Mafic Complex																			
ERP-1	RS92ER1	160	1.863	168.0	0.0321	0.7030329	0.70296	3.034	9.091	0.2015	0.513090	8.72							
ERP-2	CJ-40A	160						0.283	0.658	0.2597	0.512965	5.09						4.5	
ERP-3	CJ-41A	160	16.000	141.7	0.3267	0.70317	0.70243	0.785	1.864	0.2544	0.513020	6.28						4.8	−59
ERP-4	CJ-41A-A	160	6.149	153.0	0.1163	0.703136	0.70287	0.536	1.339	0.2418	0.513003	6.20							
ERP-5	CJ-42A	160	15.000	143.7	0.3020	0.702652	0.70197	0.463	0.978									5.6	−43
ERP-6	CJ-42B	160																5.8	
ERP-7	CJ-43A	160	2.408	145.7	0.0478	0.702808	0.70270	0.445	1.000	0.2688	0.513069	6.94							
ERP-8	CJ-43C	160	23.000	269.0	0.2474	0.703149	0.70259											5.7	−43
ERP-9	RS92ER2	160	6.000	133.0	0.1215														

Table 4. (continued)

Sample	Field Sample	Age, Ma	Rb, ppm	Sr, ppm	$\frac{^{87}Rb}{^{86}Sr}$	Measured $\frac{^{87}Sr}{^{86}Sr}$	Initial $\frac{^{87}Sr}{^{86}Sr}$	Sm, ppm	Nd, ppm	$\frac{^{147}Sm}{^{144}Nd}$	Measured $\frac{^{143}Nd}{^{144}Nd}$	$\epsilon_{Nd}(t)$	$\frac{^{206}Pb}{^{204}Pb}$	$\frac{^{207}Pb}{^{204}Pb}$	$\frac{^{208}Pb}{^{204}Pb}$	$\delta^{18}O$ Quartz	$\delta^{18}O$ Magma	WR	δD WR
ERP-10	RS92ER9	160	7.000	180.0	0.1048														
ERP-11	RS92ER15	160	9.000	177.0	0.1370											9.0	7.5		
ERP-12	RS92ER18	160	1.000	18.0	0.1497														
ERP-13	RS92ER28	160	7.000	160.0	0.1179														
ERP-14	RS92SC1	160	16.000	141.0	0.3057											8.6	7.1		
ERP-15	RS92SC7	160	13.721	150.9	0.2630	0.7040478	0.70345	1.137	3.833	0.1791	0.512964	6.73				8.7	7.2		
ERP-16	DR-1169A	160	14.000	179.0	0.2263	0.7034	0.70289											5.3	−45
ERP-17	DR-1161C	160	12.000	180.0	0.1929	0.70333	0.70289											5.7	−59
GH-1	GH-1 (CJ)	160	12.000	112.0	0.3100	0.70378	0.70307											5.6	−45
GH-2	SH-4 (CJ)	160																6.5	−48
GH-3	CJ-21 GH	160	2.603	118.0	0.0638	0.703732	0.70359	1.394	4.340	0.1939	0.513022	7.55						5.6	−53
GH-4	CJ-22	160																5.7	
GH-5	CJ-24	160																6.1	
GH-6	CJ-25	160	27.000	285.0	0.2741	0.7033	0.70268											6.0	−53
GH-7	CJ-27	160																6.8	
GH-8	CJ-28 GH	160	2.968	156.2	0.0550	0.703618	0.70349	0.752	2.279									5.7	−57
GH-9	CJ-29	160																6.4	
GH-10	RS92CV5	160	3.000	106.0	0.0762														
GH-11	RS92CV6	160	3.000	106.0	0.0762											8.9	7.4		
GH-12	DR-139	160	18.000	215.0														7.7	−47
GH-13	DR-1062	160	14.000	106.0														6.8	−50
LQ-1	LQ-1 (CJ)	160																6.1	−51
LQ-2	CJ-1F	160																6.2	−42
LQ-3	CJ-1UF LQ	160	18.000	129.0	0.4037	0.70272	0.70180											5.8	−56
LQ-4	CJ-2 LQ	160	3.282	174.5	0.0544	0.70337	0.70325	1.635	4.730	0.2087	0.513049	7.78						5.8	−44
LQ-5	CJ-3	160																	
LQ-6	SH-6 (CJ)	160	17.000	143.0	0.3439	0.70361	0.70283											5.9	−36
LQ-7	SJB-1 (CJ)	160																	
LQ-8	RS92CH1	160	12.000	213.0	0.1518											8.5	7.0		
LQ-9	RS92SJ1	160	1.000	135.0	0.0200														
LQ-10	DR-588A	160	13	153														4.1	−53

aRb, Sr, Sm, and Nd concentrations are determined by isotope dilution mass spectrometry at University of Wisconsin-Madison. Initial $^{87}Sr/^{86}Sr$ and $\epsilon_{Nd}(t)$ are calculated from measured whole rock values using the U/Pb zircon crystallization age determined for each sample; all mafic basement terrane (ERP-GH-LQ) samples are reduced to 160 Ma. Pb is corrected for mass fractionation of 0.1% per amu. Sr mass fractionation corrected to $^{86}Sr/^{88}Sr = 0.1194$ and Nd mass fractionation corrected to $^{146}Nd/^{144}Nd = 0.7219$. $\delta^{18}O_{magma}$ (per mil relative to SMOW) is calculated as $\delta^{18}O_{qtz} - 1.5‰$.

Figure 3. *Tera and Wasserburg* [1972] U/Pb concordia plot of KCGR clast zircons. Numbers refer to sample numbers that have "KCGR" prefix (see Table 2). Age uncertainties are significantly smaller than the symbol size for most zircon fractions. Zircon fractions from most clasts have complex discordance patterns reflecting both inheritance (e.g., KCGR-1, KCGR-8, and KCGR-11) and Pb loss (e.g., KCGR-13 and KCGR-18). The majority of KCGR clasts are interpreted to have crystallized at circa 100 Ma. Data are from Table 2.

eastern batholithic character are thrust over autochthonous gabbroic rocks that have oceanic affinities along the Pastoria thrust [*Ross*, 1989]. In the Gabilan Range (now displaced ∼315 km to the northwest in the central Salinian block), an analogous relation exists between the continental granitic rocks of the range and the oceanic

Logan Gabbro, separated by the Vergeles-Zayante fault [*Ross*, 1984].

4.1.1. Correlation of Continental (KCGR) Clasts

[22] The most compelling similarities between the KCGR clasts and granites of the reconstructed Sierran tail region are their continental isotopic compositions. The chemical and isotopic compositions of the KCGR clasts (eastern Cordillera arc) makes it unlikely that sedimentary processes alone were responsible for transport of coarse material from an inboard segment of the batholithic belt to the forearc without incorporating a significant amount of material from the axial and outboard portions of the arc; such processes would produce clasts with a continuous range of affinities between continental and oceanic. The forearc depositional setting of the KCGR clasts, their eastern arc compositions, as well as the absence of detritus that has intermediate compositions, appears to require a tectonically displaced source terrane.

[23] Although isotopic compositions of the KCGR clasts and the Salinia-Mojave segment of the arc are very similar, a few distinguishing age and textural characteristics require explanation. The presence of devitrified rhyolites and aphanitic granite porphyries suggests that the KCGR clasts represent a more shallow level of the crust than granites that are currently exposed in the Salinian block, western Mojave Desert, and the southernmost Sierran tail [*Schott and Johnson*, 1998a]. This difference in crustal exposure level is readily explained by additional post-Cretaceous uplift and erosion of the Salinia-Mojave source terranes [*Pickett and Saleeby*, 1993]. The age range of KCGR clasts corresponds broadly to that of the California batholiths, although the 125 Ma age for clast KCGR-9 is unusual for a rock that has an initial $^{87}Sr/^{86}Sr > 0.706$; most of the early Cretaceous plutons in the batholith are intruded into the western side of the arc and have initial $^{87}Sr/^{86}Sr < 0.706$ [*Chen and Moore*, 1982; *Chen and Tilton*, 1991]. In addition, the estimated 85 Ma age for clast KCGR-1
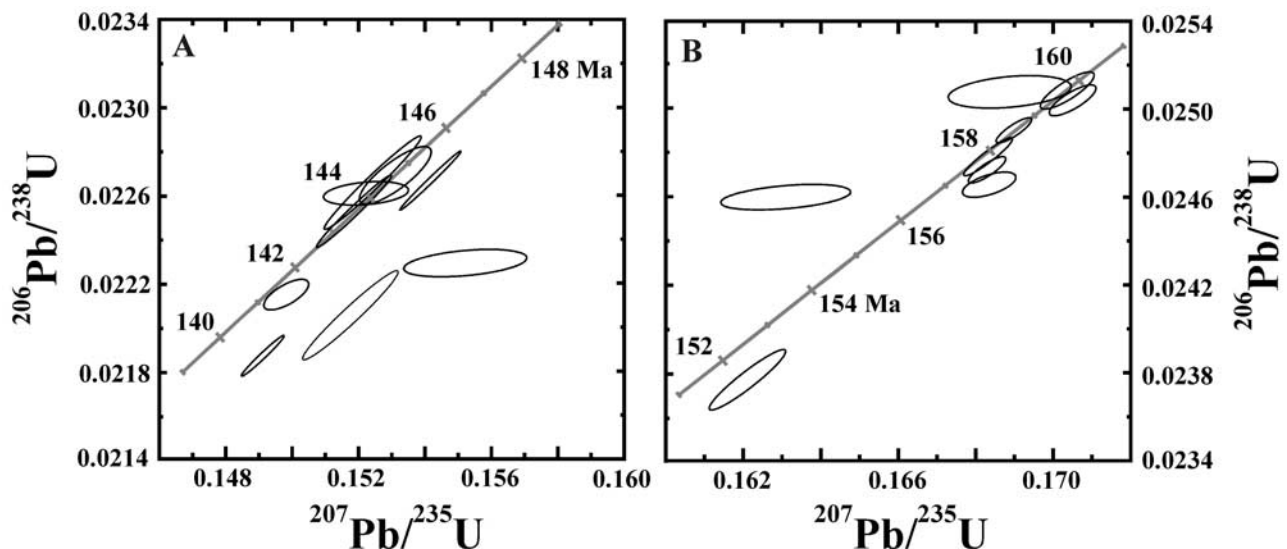
Figure 4. Conventional U/Pb concordia plots of JOGD clast zircon fractions: (a) ∼145 Ma clast ages and (b) ∼160 Ma clast and basement ages. Data are from Table 2.
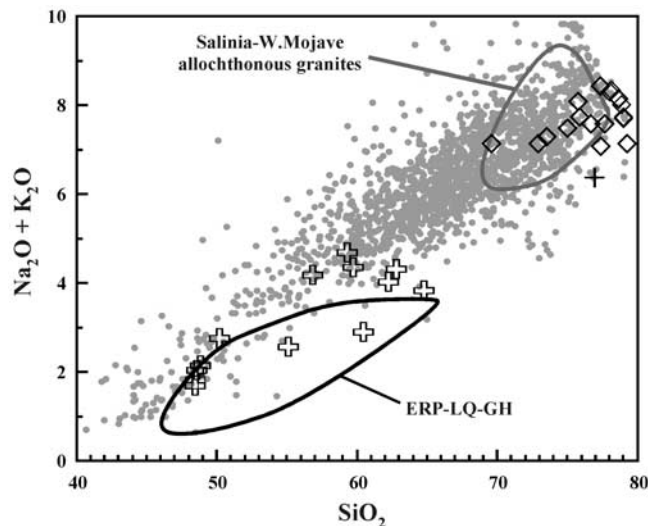
Figure 5. SiO$_2$ versus (Na$_2$O + K$_2$O) (major elements normalized to 100% anhydrous). KCGR clasts (diamonds); JOGD gabbroic clasts (open pluses); JOGD granitoid clast (pluses); and Cretaceous Cordilleran granitoids (small shaded circles; data sources given by *Schott and Johnson* [2001]). Note that KCGR clasts are unusually SiO$_2$-rich compared to most Cretaceous Cordilleran granitoids; however, there is no depletion in the alkalis that would suggest alkali mobility. Data for this study are given in Table 3.

(projected lower intercept) is remarkable in that it is relatively close to the depositional age of the rock (Maastrichtian, probably about 75 Ma), suggesting rapid uplift, erosion, and displacement of the parent body. Granitic rocks of this age form the last voluminous magmatic pulse in the Salinian block and eastern Sierra Nevada Batholith [*Stern et al.*, 1981; *Chen and Moore*, 1982; *Mattinson*, 1990; *Coleman et al.*, 1992].

4.1.2. Correlation of Oceanic (JOGD) Clasts

[24] Mafic terranes exposed in the California Coast Ranges, western Sierra Nevada, or Klamath Mountains are unlikely sources for the JOGD clasts. Although the Coast Range Ophiolite is a good match for the JOGD clasts in terms of age [*Hopson et al.*, 1981] and geochemical affinities [*Shervais*, 1990], none of the clasts at Gualala could represent the high levels of an ophiolite, which would include rock types such as cherts or shales, or igneous rocks such as pillow basalts and sheeted dikes. Furthermore, the Coast Range Ophiolite is overlain by Upper Jurassic through Upper Cretaceous sediments of the Great Valley group, and was probably not exposed at the time of deposition of the Gualala Formation [*Ingersoll*, 1983]. The Franciscan Complex is inappropriate as a source for three reasons: it lacks significant exposures of gabbro [*Shervais*, 1990]; its MORB-like geochemical characteristics are unlike the oceanic arc compositions of the JOGD clasts [*Shervais*, 1990]; and finally, distinctive Franciscan lithologies such as chert, serpentinite, and jadeite-bearing metamorphic rocks are absent in the Gualala clast assemblage [*Wentworth*, 1966]. Peridotite to diorite complexes of the Sierra Nevada and Klamath

Mountains [*Snoke et al.*, 1982] have the appropriate age and general composition, but there is no evidence that these complexes (where currently exposed) are of sufficient areal extent or proximity to the forearc to be a viable source for large clasts.

[25] Correlation of Gualala gabbroic clasts with the mafic complex at Eagle Rest Peak and its offset counterparts at Logan Quarry and Gold Hill (ERP-LQ-GH) was proposed by *Ross* [1970] and *Ross et al.* [1973] but questioned by *James et al.* [1993]. Neither the JOGD clasts nor the rocks at ERP-LQ-GH is enriched in TiO$_2$ with increasing FeO*/MgO, suggesting that both originated in a primitive oceanic arc setting. Oceanic Nd isotope compositions, as well as H-O isotope variations that indicate seawater hydrothermal alteration, are also common to ERP-GH-LQ and Gualala. Given the inferred primary crystallization age ($\geq$165 Ma) for the mafic clasts studied by *James et al.* [1993] and the ages for the JOGD clasts determined in this study (140–159 Ma), it is likely that ages of the source terrane(s) of the mafic Gualala clasts are quite variable. Although the ages for ERP-LQ-GH overlap those of the Gualala mafic clasts, we concur with all previous workers [*Ross*, 1970; *Ross et al.*, 1973; *James et al.*, 1993] that ERP-LQ-GH is probably a small surface exposure of a widespread mafic basement terrane that was exposed as the source for gabbroic detritus during the Late Cretaceous that was subsequently covered by younger sediments. This mafic basement terrane is presumed to underlie portions of the southern San Joaquin Valley, northern Salinian block, and western Mojave Desert [*Ross and McCulloch*, 1979; *Ross*, 1989], and may have been quite extensively exposed during the Late Cretaceous, which may decrease the apparent ~100–200 km travel
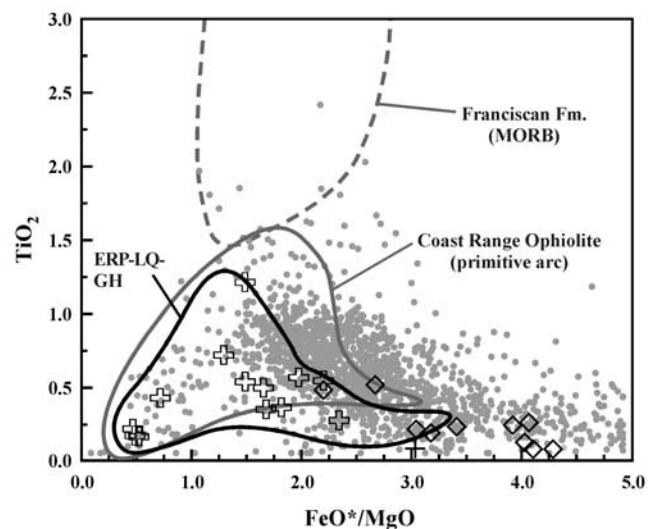
Figure 6. FeO*/MgO versus TiO$_2$. Symbols are as in Figure 5. JOGD clasts have a compositional range very similar to the mafic basement terrane at ERP-LQ-GH. Both lack TiO$_2$ enrichment with increasing FeO*/MgO ratio that is characteristic of MORB. Data for this study are from Table 3. Fields for Coast Range Ophiolite and Franciscan are from *Shervais* [1990]. Data sources for Cretaceous Cordilleran granitoids are given by *Schott and Johnson* [2001].
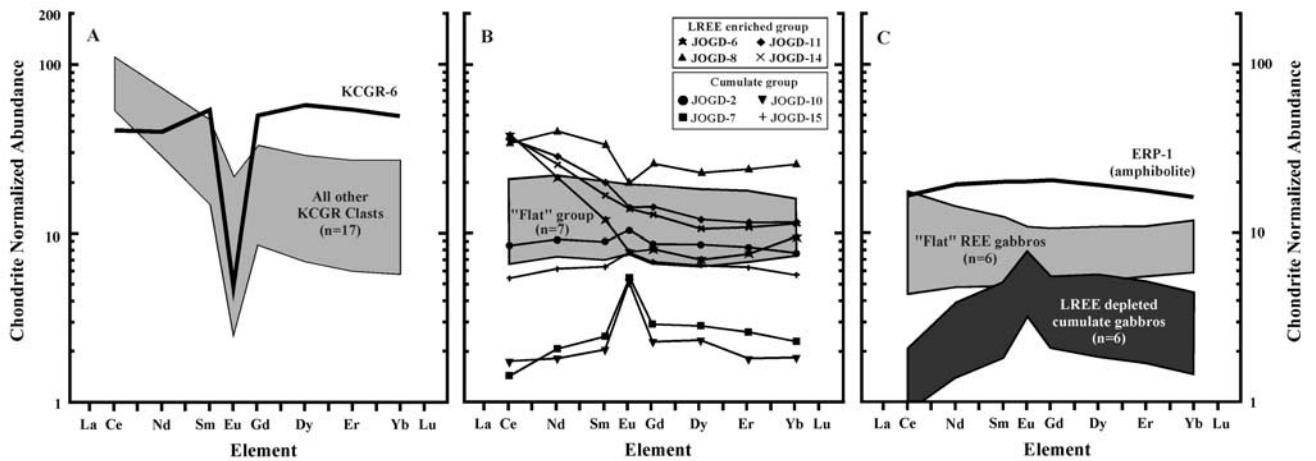
Figure 7. Chondrite normalized REE diagrams for (a) KCRG clasts, (b) JOGD clasts, and (c) ERP-GH-LQ mafic complex. See discussion in text. Data are from Table 3.

distances for the mafic Gualala clasts inferred from palinspastic reconstructions (Figure 11).

4.2. Tectonic Controls on Late Cretaceous-Paleocene Sedimentation

[26] Late Cretaceous to Paleocene sedimentation in the Gualala basin is inferred to reflect tectonic events associated with the collapse of the Salinia-Mojave segment of the Cretaceous Cordilleran arc [*Schott and Johnson*, 1998a]. The basal Stewarts Point Member conglomerate of Campanian age is a massive cobble- and boulder-dominated assemblage that is up to one kilometer thick; KCGR clasts comprise the majority of the clast population. Initiation of KCGR conglomerate sedimentation in the basin has been interpreted to reflect the tectonic emplacement of an allochthon that was derived from the inboard portions of the Cordilleran arc, into a position that was adjacent to the forearc [*Schott and Johnson*, 1998a, 1998b]. Initiation of the arc collapse event is constrained to be circa 80 Ma [*Schott and Johnson*, 1998a, 1998b].

[27] Data for the JOGD clasts permit two possible source terranes that allow differing tectonic interpretations. One possibility is that the upsection increase in the proportion of JOGD clasts reflects progressive erosional unroofing of the granitic allochthon and exposure of the tectonically underlying Jurassic mafic basement terrane. This mafic basement terrane may be the sole source for Anchor Bay gabbroic clasts if its currently buried portions include circa 145 Ma rocks (similar to the Coast Range Ophiolite). Alternatively, the Anchor Bay gabbroic clasts may be derived from an oceanic arc terrane that was exotic to North America. In the exotic arc model, the upsection increase in gabbroic clasts in the Gualala Formation may be the result of accretion of this arc to the North American continental margin during the latest Cretaceous to Paleocene. Finally, it is possible that the mafic conglomerate at Gualala contains both circa 160 Ma North American basement (ERP-GH-LQ) and circa 145 Ma exotic arc components.

[28] The overall decrease in conglomerate abundance and clast size upward through the Late Cretaceous and early Tertiary sections at Gualala may reflect a decrease in

topography in the source area due to continued erosion or relative transport of the basin away from the Late Cretaceous sediment source area. The presence of a first-generation clast of Late Jurassic (~145 Ma) oceanic gabbro in the overlying Eocene German Rancho Formation [*Schott and Johnson*, 2001] suggests that the same gabbroic source terrane contributed sediment to the basin during both the Maastrichtian and early Eocene, implying that translation of
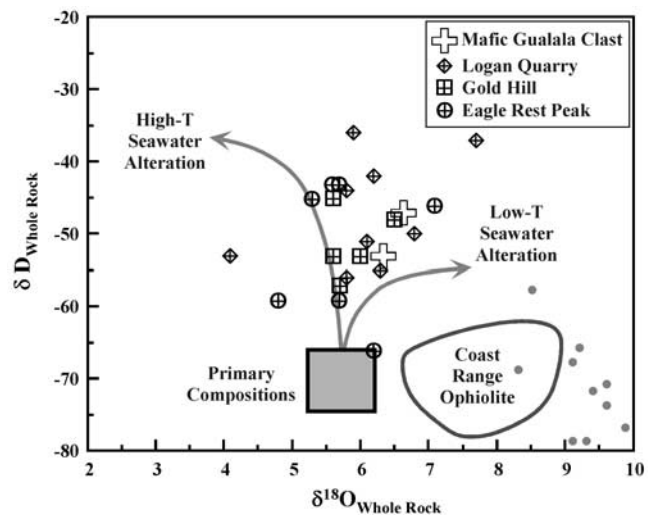
Figure 8. The δD-$\delta^{18}O$ variations for whole rock ERP-LQ-GH basement samples and two JOGD clasts. All δD values are significantly higher than those of primary igneous compositions, indicating hydrothermal interaction with fluids that contained high-δD values, such as seawater ($\delta D \sim 0‰$), rather than meteoric waters, which have lower δD values. A seawater hydrothermal alteration trend is shared among ERP, GH, and LQ, as well as the two JOGD clasts. Data for samples from this study are from Table 4. Field for the Coast Range Ophiolite is from *Magaritz and Taylor* [1976]. Small gray circles are data from Salinian plutons from *Masi et al.* [1981].
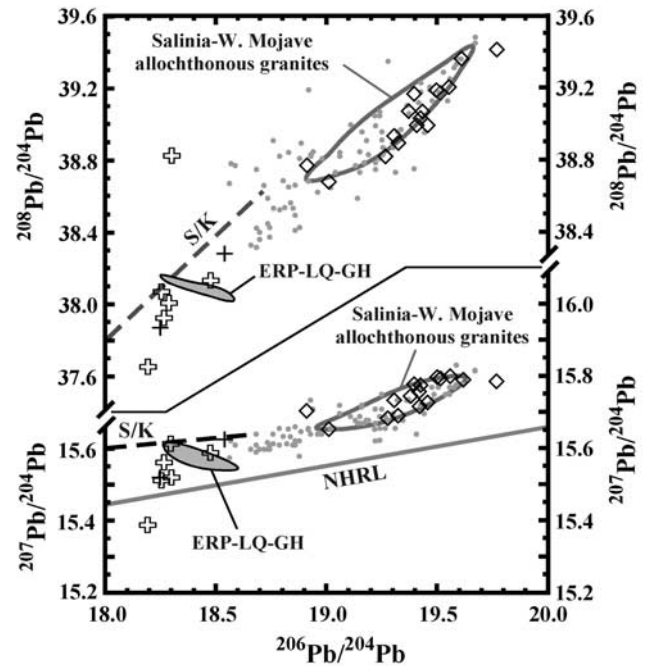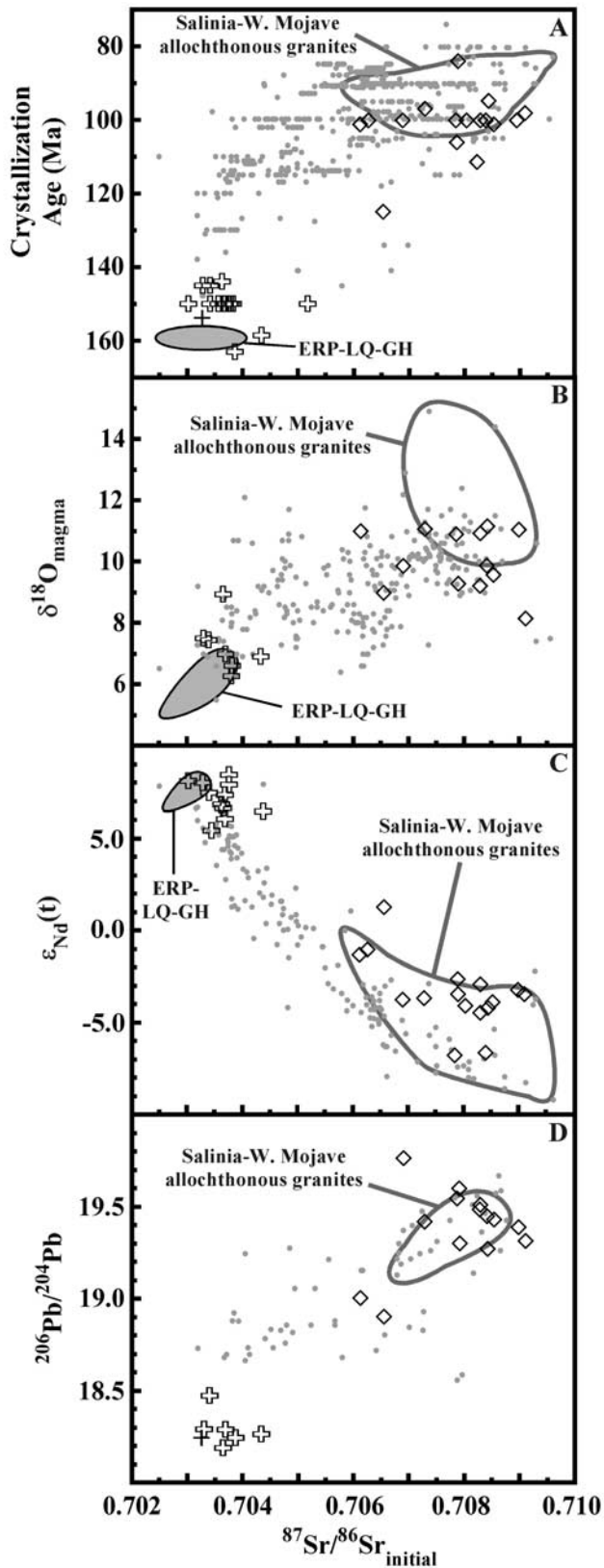
Figure 10. Pb isotope variation diagrams: (a) $^{207}Pb/^{204}Pb$ versus $^{206}Pb/^{204}Pb$ and (b) $^{208}Pb/^{204}Pb$ versus $^{206}Pb/^{204}Pb$. Symbols are as in Figure 5. JOGD clasts illustrate a relatively steep trend in that may reflect assimilation and mixing with an older Pb component that had a low Th/U ratio. S/K is *Stacey and Kramers* [1975] average crustal growth curve. NHRL is Northern Hemisphere reference line [*Hart*, 1984]. The moderately high $^{207}Pb/^{204}Pb$ ratios of the KCRG clasts overlap those of the Salinia-western Mojave plutons. Data for samples from this study are from Table 4. Data sources for Cretaceous plutonic rocks are given by *Schott and Johnson* [2001].

the basin during the early Paleogene was minimal (less than tens of kilometers).

4.3. Pre-Neogene Basement Relations in the Northern Salinian Block−Southern Sierran Nevada Batholith−Western Mojave Desert Region

[29] The subsurface extent, age, and tectonic affinity of the mafic basement terrane that is exposed in ERP-LQ-GH are uncertain, although the range in age of up to 25 m.y. of the mafic Gualala clasts suggests the source region(s) must have been more extensive than the exposed extent of

Figure 9. Variations initial $^{87}Sr/^{86}Sr$ ratios for Gualala clasts relative to (a) U/Pb zircon ages, (b) $\delta^{18}O$ values, (c) $\varepsilon_{Nd}(t)$ values, and (d) $^{206}Pb/^{204}Pb$ ratios. Symbols are as in Figure 5. Note particularly the unusual enrichment in $^{87}Sr/^{86}Sr_{init}$ at a given $\varepsilon_{Nd}(t)$, a feature that is relatively unique to KCGR clasts and basement samples of allochthonous granites from the Salinian block and western Mojave Desert. JOGD clasts are generally a good match for the oceanic basement terrane at ERP-LQ-GH, though some JOGD clasts may have enriched $^{87}Sr/^{86}Sr_{init}$ ratios due to limited hydrothermal alteration by seawater. Data for samples from this study are from Table 4.
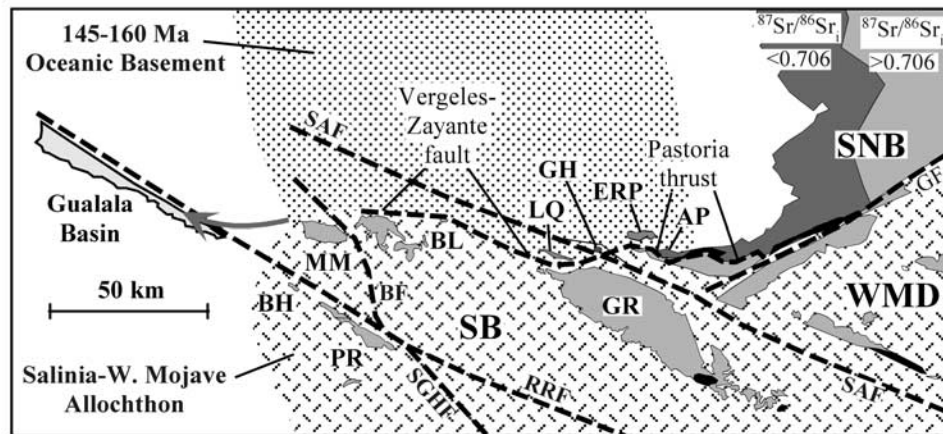
Figure 11. Pre-Neogene palinspastic reconstruction of the southernmost Sierra Nevada Batholith (SNB), north central Salinian block (SB), and westernmost Mojave Desert (WMD) region illustrating the juxtaposition of interior arc continental granitoids of the Salinia-western Mojave Allochthon (hachured pattern) with 145–160 Ma oceanic basement (stippled pattern) in a location adjacent to the forearc depositional location of the Gualala basin. The Pastoria thrust and Vergeles-Zayante fault mark this tectonic boundary in the southernmost SNB and northern Salinian block, respectively. North is generally toward the top of the diagram but cannot be well constrained. Schematic locations of faults with Neogene offset are abbreviated as follows: SAF, San Andreas fault; GF, Garlock Fault; SGHF, San Gregorio-Hosgri fault; RRF, Reliz-Rinconada fault; BF, Butano fault. Modified from *James* [1992] and *Powell* [1993]. Granitic basement in the Salinian block: BH, Bodega Head; MM, Montara Mountain; BL, Ben Lomond; PR, Point Reyes; GR, Gabilan Range. Mafic basement terrane exposures: LQ, Logan Quarry; GH, Gold Hill; ERP, Eagle Rest Peak; AP, Antimony Peak.

ERP-LQ-GH. Extension of the ERP-LQ-GH terrane may be reflected in the strong positive magnetic anomaly that extends westward beneath the Butano basin in the Salinian block, and north and east beneath the southern San Joaquin Valley [*Jachens et al.*, 1998]. Mafic basement is inferred to underlie the granites of the central Salinian block at a depth of ~13 km [*Ross and McCulloch*, 1979]. No samples that have ages of 145 Ma have yet been recovered from the buried portions of this terrane, but the mafic tonalite of Antimony Peak [*Ross*, 1989], located in the westernmost Sierran tail and structurally below the Pastoria thrust just a few kilometers south of the Eagle Rest Peak (Figure 11), has been dated at 131 Ma [*James*, 1986].

[30] Conglomerate provenance data presented here constrain the depositional location of the basin to have been adjacent to North America at the latitude of the southernmost Sierra Nevada (and palinspastically restored northern Salinian block) during the Late Cretaceous. The depositional location of the Gualala basin is only broadly constrained, however, because the age and compositional variability of the mafic basement terrane, as well as the Late Cretaceous location of its tectonic boundary with Salinian granites, are poorly known. The contact between the allochthonous continental granite-rhyolite terrane and the underlying oceanic mafic terrane may have been a laterally extensive, originally subhorizontal detachment surface [*Silver*, 1982, 1983; *Silver and Mattinson*, 1986]. Remnants of this terrane boundary are preserved in the Sierran tail as the Pastoria thrust and in the Salinian block as the Vergeles-Zayante fault [*Ross*, 1984, 1989]. Our results therefore suggest that an Upper Cretaceous detachment in the Sierran batholith best explains the two populations of Gualala clasts, and this and

related structures were subsequently modified by Neogene deformation associated with the San Andreas fault system [*Ross*, 1984, 1989].

[31] The tectonic reconstruction favored by our data (Figure 11) is at odds with an inferred low-latitude origin for the Gualala basin [*Kanter and Debiche*, 1985], where shallow magnetic inclinations suggested between 4000 and 1800 km of northward transport of the basin relative to cratonic North America. These magnitudes of transport are far in excess of those suggested by the provenance data presented here (~450–650 km), even after a component of northward motion east of the San Andreas fault system [*Dickinson and Wernicke*, 1997] is taken into account. We therefore suggest that the paleomagnetic data from the Gualala basin overestimate the extent of northward transport of the basin. Uncertainties due to compaction and deformation seem likely explanations for the excessive transport distances inferred from paleomagnetic data [e.g., *James et al.*, 1993; *Kodama and Davi*, 1995]. Paleontologic evidence that implies a low-latitude Upper Cretaceous origin for beds in the Gualala Formation includes the rudistid bivalve *Coralliochama orcutt*, which has subtropical Tethyan affinities [*Elder et al.*, 1998]. Such evidence is unlikely to place rigorous constraints on paleolatitudes because the rudist fragments in the Anchor Bay member conglomerate beds are detrital in origin, and the same beds also contain Paleocene foraminifera [*McDougall*, 1998].

5. Summary

[32] The Late Cretaceous depositional location of the Gualala basin appears to reflect the most outboard or

westernmost record of sedimentation in the Cordilleran arc complex of California after cessation of Sierra Nevada batholith magmatism and, as such, potentially records tectonic events whose record is not preserved in the major, interior portions of the arc. Detailed U/Pb zircon ages, geochemical, and isotopic data for conglomerate clasts identify two groups that were deposited contemporaneously: (1) the KCGR suite comprising granitic and rhyolitic clasts that have mid-Cretaceous ages and continental chemical and isotopic compositions, that were derived from a fragment of the shallow levels of the eastern (interior) portion of the Cretaceous Cordilleran magmatic arc, and (2) the JOGD suite comprising gabbroic and quartz dioritic clasts that have Late Jurassic crystallization ages and chemical and isotopic compositions that indicate derivation from an oceanic arc. The strong isotopic and compositional contrast between these suites and their common occurrence in individual beds imply a tectonic juxtaposition of their sources in a near-forearc setting prior to sedimentation, which most likely occurred through westward collapse of the eastern Sierra-Mojave arc along a major detachment structure. The structures that were associated with juxtaposition of the eastern continental and western oceanic sections of the arc are likely to have produced weaknesses in the lithosphere that were later exploited by transform motion along the San Andreas system. Correlation of the Late Cretaceous conglomerate clast assemblage with a source on the North American continent at the latitude of the southernmost Sierra Nevada provides strong evidence that the terranes of western California that lie west of the San Andreas transform system are not exotic or far traveled, contrary to paleomagnetic data that imply thousands of kilometers of northward transport since the Eocene.

References

Bateman, P. C. (1992), Plutonism in the central part of the Sierra Nevada Batholith, California, *U.S. Geol. Surv. Prof. Pap., 1483*, 186 pp., 2 sheets.

Burnham, K. (1998), Preliminary comparison and correlation of two Cretaceous conglomerates, the strata of Anchor Bay and an unnamed unit in the Pilarcitos block, across the San Gregorio and San Andreas faults, in *Geology and Tectonics of the Gualala Block, Northern California*, edited by W. P. Elder, *Publ. 84*, pp. 95–119, Pac. Sect., SEPM, Golden Gate, Calif.

Chen, J. H., and J. G. Moore (1982), Uranium-lead isotopic ages from the Sierra Nevada batholith, California, *J. Geophys. Res., 87*(B6), 4761–4784.

Chen, J. H., and H. F. Shaw (1982), Pb-Nd-Sr isotopic studies of California ophiolites, *Geol. Soc. Am. Abstr. Programs, 14*(7), 462.

Chen, J. H., and G. R. Tilton (1991), Applications of lead and strontium isotopic relationships to the petrogenesis of granitoid rocks, central Sierra Nevada Batholith, California, *Geol. Soc. Am. Bull., 103*, 439–447.

Church, S. E. (1976), The Cascade Mountains revisited: A re-evaluation in light of new lead isotopic data, *Earth Planet. Sci. Lett., 29*, 175–188.

Coleman, D. C., T. P. Frost, and A. F. Glazner (1992), Evidence from the Lamarck Granodiorite for rapid Late Cretaceous crust formation in California, *Science, 258*, 1924–1926.

Cowan, D. S. (1994), Alternative hypotheses for the Mid-Cretaceous paleogeography of the Western Cordillera, *GSA Today, 4*, 181, 184–186.

Cowan, D. S., M. T. Brandon, and J. I. Garver (1997), Geological tests of hypotheses for large coastwise displacements: A critique illustrated by the Baja British Columbia controversy, *Am. J. Sci., 297*, 117–173.

DePaolo, D. J. (1981), A neodymium and strontium isotopic study of the Mesozoic calc-alkaline granitic batholiths of the Sierra Nevada and Peninsular Ranges, California, *J. Geophys. Res., 86*(B11), 10,470–10,488.

Dickinson, W. R., and R. F. Butler (1998), Coastal and Baja California paleomagnetism reconsidered, *Geol. Soc. Am. Bull., 110*, 1268–1280.

Dickinson, W. R., and B. P. Wernicke (1997), Reconciliation of San Andreas slip discrepancy by a combination of interior Basin and Range extension and transrotation near the coast, *Geology, 25*, 663–665.

Dodge, F. C. W., B. P. Fabbi, and D. C. Ross (1970), Potassium and rubidium in granitic rocks of central California, *U.S. Geol. Surv. Prof. Pap., 700D*, 108–115.

Elder, W. P., L. R. Saul, and C. L. Powell II (1998), Late Cretaceous and Paleogene molluscan fossils of the Gualala block and their paleogeographic implications, in *Geology and Tectonics of the Gualala Block, Northern California*, edited by W. P. Elder, *Publ. 84*, pp. 149–167, Pac. Sect., SEPM, Golden Gate, Calif.

Fleck, R. J., and R. E. Criss (1985), Strontium and oxygen isotopic variations in Mesozoic and Tertiary plutons of central Idaho, *Contrib. Mineral. Petrol., 90*, 291–308.

Graham, S. A., R. G. Stanley, J. V. Bent, and J. B. Carter (1989), Oligocene and Miocene paleogeography of central California and displacement along the San Andreas Fault, *Geol. Soc. Am. Bull., 101*, 711–730.

Hart, S. R. (1984), A large-scale isotope anomaly in the Southern Hemisphere mantle, *Nature, 309*, 753–757.

Hart, S. R., D. C. Gerlach, and W. M. White (1986), A possible new Sr-Nd-Pb mantle array and consequences for mantle mixing, *Geochim. Cosmochim. Acta, 50*, 1551–1557.

Hawkins, J. W., S. H. Bloomer, C. A. Evans, and J. T. Melchior (1984), Evolution of intra-oceanic arc-trench systems, *Tectonophysics, 102*, 175–205.

Hopson, C. A., J. M. Mattinson, and E. A. Pessagno Jr. (1981), Coast Range ophiolite, western California, in *The Geotectonic Development of California*, Rubey Vol. I, edited by W. G. Ernst, pp. 418–510, Prentice-Hall, Old Tappan, N. J.

Ingersoll, R. V. (1983), Petrofacies and provenance of late Mesozoic forearc basin, northern and central California, *AAPG Bull., 67*, 1125–1142.

Jachens, R. C., C. M. Wentworth, and R. J. McLaughlin (1998), Pre-San Andreas location of the Gualala block inferred from magnetic and gravity anomalies, in *Geology and Tectonics of the Gualala Block, Northern California*, edited by W. P. Elder, *Publ. 84*, pp. 27–63, Pac. Sect., SEPM, Golden Gate, Calif.

James, E. W. (1986), U/Pb age of the Antimony Peak Tonalite and its relation to Rand Schist in the San Emigdio Mountains, California, *Geol. Soc. Am. Abstr. Programs, 18*(2), 121.

James, E. W. (1992), Cretaceous metamorphism and plutonism in the Santa Cruz Mountains, Salinian block, California, and correlation with the southernmost Sierra Nevada, *Geol. Soc. Am. Bull., 104*, 1326–1339.

James, E. W., D. L. Kimbrough, and J. M. Mattinson (1993), Evaluation of displacements of pre-Tertiary rocks on the northern San Andreas fault using U-Pb zircon dating, initial Sr, and common Pb isotopic ratios, in *The San Andreas Fault System: Displacement, Palinspastic Reconstruction, and Geologic Evolution*, edited by R. E. Powell, R. J. Weldon II, and J. C. Matti, *Mem. Geol. Soc. Am., 178*, 257–271.

Kanter, L. R., and M. Debiche (1985), Modeling the motion histories of the Point Arena and central Salinia terranes, in *Tectonostratigraphic Terranes of the Circum-Pacific region*, edited by D. G. Howell, pp. 226–238, Circum-Pac. Counc. for Energy and Miner. Resour., Houston, Tex.

Kistler, R. W., and Z. E. Peterman (1973), Variations in Sr, Rb, K, Na, and initial $^{87}Sr/^{86}Sr$ in Mesozoic granitic rocks and intruded wall rocks in central California, *Geol. Soc. Am. Bull., 84*, 3489–3512.

Kistler, R. W., and Z. E. Peterman (1978), Reconstruction of crustal blocks of California on the basis of initial strontium isotopic compositions of Mesozoic granitic rocks, *U.S. Geol. Surv. Prof. Pap., 1071*, 17 pp.

Kistler, R. W., and D. C. Ross (1990), A strontium isotopic study of plutons and associated rocks of the southern Sierra Nevada and vicinity, California, *U.S. Geol. Surv. Bull.*, *1920*, 20 pp.

Kistler, R. W., Z. E. Peterman, D. C. Ross, and D. Gottfried, (1973), Strontium isotopes and the San Andreas fault, in *Conference on Tectonic Problems of the San Andreas Fault System, Proceedings*, Stanford Univ. Publ. Geol. Sci., *13*, 339–347.

Kodama, K. P., and J. M. Davi (1995), A compaction correction for the paleomagnetism of the Cretaceous Pigeon Point Formation of California, *Tectonics*, *14*, 1153–1164.

Krogh, T. E. (1973), A low-contamination method for hydrothermal decomposition of zircon and extraction of U and Pb for isotopic age determination, *Geochim. Cosmochim. Acta*, *37*, 485–494.

Lin, P. N., R. J. Stern, J. Morris, and S. H. Bloomer (1990), Nd- and Sr-isotopic compositions of lavas from the northern Mariana and southern volcano arcs; implications for the origin of island arc melts, *Contrib. Mineral. Petrol.*, *105*, 381–392.

Loomis, K. B., and J. C. Ingle Jr. (1994), Subsidence and uplift of the Late Cretaceous-Cenozoic margin of California: New evidence from the Gualala and Point Arena basins, *Geol. Soc. Am. Bull.*, *106*, 915–931.

Ludwig, K. R. (1989), PBDAT for MS-DOS a computer program for IBM-PC compatibles for processing raw Pb-U-Th isotope data version 1.06, *U.S. Geol. Surv. Open File Rep., 88-542*.

Magaritz, M., and H. P. Taylor Jr. (1976), Oxygen, hydrogen, and carbon isotope studies of the Franciscan Formation, Coast Ranges, California, *Geochim. Cosmochim. Acta*, *40*, 215–234.

Masi, U., J. R. O'Neil, and R. W. Kistler (1981), Stable isotope systematics in Mesozoic granites of central and northern California and southwestern Oregon, *Contrib. Mineral. Petrol.*, *76*, 116–126.

Mattinson, J. M. (1990), Petrogenesis and evolution of the Salinian magmatic arc, in *The Nature and Origin of Cordilleran Magmatism*, edited by J. L. Anderson, *Mem. Geol. Soc. Am.*, *174*, 237–250.

McCulloch, M. T., R. T. Gregory, G. J. Wasserburg, and H. P. Taylor Jr. (1981), Sm-Nd, Rb-Sr, and $^{18}O/^{16}O$ isotopic systematics in an oceanic crustal section: Evidence from the Samail Ophiolite, *J. Geophys. Res.*, *86*, 2721–2735.

McDougall, K. (1998), Paleogene foraminifera of the Gualala block and their relation to local and global events, in *Geology and Tectonics of the Gualala Block, Northern California*, edited by W. P. Elder, *Publ. 84*, pp. 169–188, Pac. Sect., SEPM, Golden Gate, Calif.

Miller, C. F., and D. W. Mittlefehldt (1982), Depletion of light rare-earth elements in felsic magmas, *Geology*, *10*, 129–133.

Miyashiro, A. (1973), The Troodos ophiolitic complex was probably formed in an island arc, *Earth Planet. Sci. Lett.*, *19*, 218–224.

Phillips, J. R., R. C. Erickson, and T. B. Anderson (1998), Geochemical analysis of basaltic rocks near Black Point, northern Sonoma County, California, in *Geology and Tectonics of the Gualala Block, Northern California*, edited by W. P. Elder, *Publ. 84*, pp. 65–74, Pac. Sect., SEPM, Golden Gate, Calif.

Pickett, D. A., and J. B. Saleeby (1993), Thermobarometric constraints on the depth of exposure and conditions of plutonism and metamorphism at deep levels of the Sierra Nevada Batholith, Tehachapi Mountains, California, *J. Geophys. Res.*, *98*, 609–629.

Powell, R. E. (1993), Balanced palinspastic reconstruction of pre-late Cenozoic paleogeography, southern California: Geologic and kinematic constraints on evolution of the San Andreas fault system, in *The San Andreas Fault System: Displacement, Palinspastic Reconstruction, and Geologic Evolution*, edited by R. E. Powell, R. J. Weldon II, and J. C. Matti, *Mem. Geol. Soc. Am.*, *178*, 1–106.

Reitz, A. (1986), The geology and petrology of the northern San Emigdio plutonic complex, San Emigdio Mountains, southern California, M.A. thesis, 80 pp., Univ. of Calif., Santa Barbara.

Ross, D. C. (1970), Quartz gabbro and anorthositic gabbro: Markers of offset along the San Andreas fault in the California Coast Ranges, *Geol. Soc. Am. Bull.*, *81*, 3647–3662.

Ross, D. C. (1982), Results of instrumental neutron activation analyses for selected plutonic samples from the Salinian block, California Coast Ranges, *U.S. Geol. Surv. Open File Rep.*, *82-935*, 17 pp.

Ross, D. C. (1984), Possible correlations of basement rocks across the San Andreas, San Gregorio-Hosgri, and Rinconada-Reliz-King faults, California, *U.S. Geol. Surv. Prof. Pap.*, *1317*, 37 pp.

Ross, D. C. (1989), The metamorphic and plutonic rocks of the southernmost Sierra Nevada, California, and their tectonic framework, *U.S. Geol. Surv. Prof. Pap.*, *1381*, 159 pp., 2 sheets.

Ross, D. C., and D. S. McCulloch (1979), Cross section of the southern Coast Ranges and San Joaquin Valley from offshore Point Sur to Madera, California, *Geol. Soc. Am. Map Chart Ser.*, *MC-28H*, 4 pp., 1 sheet.

Ross, D. C., C. M. Wentworth, and E. H. McKee (1973), Cretaceous mafic conglomerate near Gualala offset 350 miles by the San Andreas fault

from oceanic crustal source, near Eagle Rest Peak, California, *U.S. Geol. Surv. J. Res.*, *1*, 45–52.

Saleeby, J. B., D. B. Sams, and R. W. Kistler (1987), U/Pb zircon, strontium, and oxygen isotopic and geochronological study of the southernmost Sierra Nevada batholith, California, *J. Geophys. Res.*, *92*, 10,443–10,466.

Schott, R. C. (2000), Provenance evolution of the Late Cretaceous - Middle Eocene Gualala basin, California: Geochronologic, geochemical, and isotopic evidence from conglomerate clasts, Ph.D. thesis, 273 pp., University of Wisconsin-Madison, Madison.

Schott, R. C., and C. M. Johnson (1998a), Sedimentary record of the Late Cretaceous thrusting and collapse of the Salinia-Mojave magmatic arc, *Geology*, *26*, 327–330.

Schott, R. C., and C. M. Johnson (1998b), Late Cretaceous to Eocene Gualala basin provenance constraints from conglomerate clasts: Implications for the origin and early evolution of the Salinian block, in *Geology and Tectonics of the Gualala Block, Northern California*, edited by W. P. Elder, *Publ. 84*, pp. 75–94, Pac. Sect., SEPM, Golden Gate, Calif.

Schott, R. C., and C. M. Johnson (2001), Garnet-bearing trondhjemite and other conglomerate clasts from the Gualala Basin, California; sedimentary record of the missing western portion of the Salinian magmatic arc?, *Geol. Soc. Am. Bull.*, *113*, 870–880.

Shervais, J. W. (1990), Island arc and ocean crust ophiolites: Contrasts in the petrology, geochemistry and tectonic style of ophiolite assemblages in the California Coast Ranges, in *Ophiolites: Oceanic Crustal Analogues*, edited by J. Malpas et al., pp. 507–520, Geol. Surv. Dep., Nicosia, Cyprus.

Silver, L. T. (1982), Evidence and a model for west-directed early to mid-Cenozoic basement overthrusting in southern California, *Geol. Soc. Am. Abstr. Programs*, *14*, 617.

Silver, L. T. (1983), Paleogene overthrusting in the tectonic evolution of the Transverse Ranges, Mojave and Salinian regions, California, *Geol. Soc. Am. Abstr. Programs*, *15*, 438.

Silver, L. T., and J. M. Mattinson (1986), "Orphan Salinia" has a home (abstract), *Eos Trans. AGU*, *67*, 1215.

Silver, L. T., H. P. Taylor Jr., and B. Chappell (1979), Some petrological, geochemical and geochronological observations of the Peninsular Ranges Batholith near the international border of the U.S.A. and Mexico, in *Mesozoic Crystalline Rocks*, edited by P. L. Abbott and V. R. Todd, pp. 83–110, San Diego State Univ., Dep. of Geol. Sci., San Diego, Calif.

Snoke, A. W., W. D. Sharp, J. E. Wright, and J. B. Saleeby (1982), Significance of mid-Mesozoic peridotitic to dioritic intrusive complexes, Klamath Mountains-western Sierra Nevada, California, *Geology*, *10*, 160–166.

Solomon, G. C. (1989), An $^{18}O/^{16}O$ study of Mesozoic and early Tertiary granitic batholiths of the southwestern North American Cordillera, Ph.D. thesis, 538 p., Calif. Inst. of Technol., Pasadena.

Solomon, G. C., and H. P. Taylor Jr. (1989), Isotopic evidence for the origin of Mesozoic and Cenozoic granitic plutons in the northern Great Basin, *Geology*, *17*, 591–594.

Stacey, J. S., and J. D. Kramers (1975), Approximation of terrestrial lead isotope evolution by a two-stage model, *Earth Planet. Sci. Lett.*, *26*, 207–221.

Steiger, R. H., and E. Jäger (1977), Subcommission on geochronology: Convention on the use of decay constants in geo- and cosmochronology, *Earth Planet. Sci. Lett.*, *36*, 359–362.

Stern, R. J., M. C. Jackson, P. Fryer, and E. Ito (1993), O, Sr, Nd and Pb isotopic composition of the Kasuga Cross-Chain in the Mariana Arc; a new perspective on the K-h relationship, *Earth Planet. Sci. Lett.*, *119*, 459–475.

Stern, T. W., P. C. Bateman, B. A. Morgan, M. F. Newell, and D. L. Peck (1981), Isotopic U-Pb ages of zircon from the granitoids of the central Sierra Nevada, California, *U.S. Geol. Surv. Prof. Pap.*, *1185*, 17 pp.

Taylor, H. P., and L. T. Silver (1978), Oxygen isotope relationships in plutonic igneous rocks of the Peninsular Ranges Batholith, southern and Baja California, in *Short Papers of the Fourth International Conference, Geochronology, Cosmochronology, Isotope Geology*, edited by R. E. Zartman, *U.S. Geol. Surv. Open File Rep., 78-701*, 423–426.

Tera, F., and G. J. Wasserburg (1972), U-Th-Pb systematics in three Apollo 14 basalts and the problem of initial Pb in lunar rocks, *Earth Planet. Sci. Lett.*, *14*, 281–304.

Wentworth, C. M. (1966), The Upper Cretaceous and lower Tertiary rocks of the Gualala area, northern Coast Ranges, California, Ph.D. thesis, 197 pp., Stanford Univ., Palo Alto, Calif.

Wentworth, C. M., D. L. Jones, and E. E. Brabb (1998), Geology and regional correlation of the Cretaceous and Paleogene rocks of the Gualala block, California, in *Geology and Tectonics of the Gualala Block, Northern California*, edited by W. P. Elder, *Publ. 84*, pp. 3–26, Pac. Sect., SEPM, Golden Gate, Calif.

Wooden, J. L., J. S. Stacey, K. A. Howard, B. R. Doe, and D. M. Miller (1988), Pb isotopic evidence for the formation of Proterozoic crust in the Southwestern United States, in *Metamorphism and Crustal Evolution of the Western United States, Rubey Vol. 7*, edited by W. G. Ernst, pp. 68–86, Prentice-Hall, Old Tappan, N. J.

Woodhead, J. D., and D. G. Fraser (1985), Pb, Sr and [10]Be isotopic studies of volcanic rocks from the northern Mariana Islands; implications for magma genesis and crustal recycling in the western Pacific, *Geochim. Cosmochim. Acta, 49*, 1925–1930.

Zindler, A., S. R. Hart, F. A. Frey, and S. P. Jacobson (1979), Nd and Sr isotope ratios and rare earth element abundances in Reykjanes Peninsula basalts: Evidence for mantle heterogeneity beneath Iceland, *Earth Planet. Sci. Lett., 45*, 249–262.

———————————

C. M. Johnson, Department of Geology and Geophysics, University of Wisconsin-Madison, Madison, WI 53706, USA. (clarkj@geology.wisc.edu)

J. R. O'Neil, Department of Geological Sciences, University of Michigan, Ann Arbor, MI 48109-1063, USA. (jro@umich.edu)

R. C. Schott, Department of Geology and Physics, Lake Superior State University, Sault Sainte Marie, MI 49783, USA. (rschott@lssu.edu)